UNITED NATIONS UNIVERSITY
GEOTHERMAL TRAINING PROGRAMME
Orkustofnun, Grensasvegur 9,
IS-108 Reykjavik, Iceland

Reports 2013
Number 30

ANALYSIS OF GEOTHERMAL CASING THINNING RATE OF LEYTE GEOTHERMAL PRODUCTION FIELD

Anthony S. Ponce
Energy Development Corporation - EDC
38/F One Corporate Center Building
Julia Vargas corner Meralco Avenue
OrtigasCenter, Pasig City, 1605
PHILIPPINES
ponce.as@energy.com.ph

ABSTRACT

Corrosion is one of the technological problems that geothermal management faces in the operation of geothermal wells. The primary cause of corrosion in geothermal wells is exposure to geothermal brine where conductive and convective heat transfer happens from the reservoir to the surface. The geothermal well supplies the motive two-phase steam fluid from the reservoir to the surface fluid collection facility, and then to the separator where steam is separate from brine. The casing of the well is the first equipment that encounters the field's geothermal fluid. The flow of geothermal brine from the reservoir causes the casing to deteriorate by way of corrosion. The impact of turbulence, corrosion and erosion significantly reduce the integrity of the casing. Thus, monitoring these facilities is vitally important to minimize the risks to geothermal operations. Caliper measurements are taken to monitor the thickness of the casing for safety and environmental concerns. The effective management of a geothermal well necessitates a very thorough knowledge of the extent to which the aforementioned factors contribute to casing degradation. In this paper, the contribution of factors affecting the thinning rate of a geothermal casing, such as temperature, flow velocity, pH, well geometry and corrosion species, was studied. The effects of several corrosive species on casings were also studied. The corrosive species and the factors affecting the thinning rate of the production wells of the Leyte geothermal production field were analysed with multiple linear regression models in order to determine the dependency of the thinning rate on these parameters. Fluid discharge measurements and sampled chemistry concentrations at the surface were simulated at downhole conditions using software HOLA and WATCH. The results were analysed statistically using ANOVA, a P value test, and multiple regression coefficients. Adjusted R^2 of the regression analysis and mean absolute percentage error (MAPE) aided in selecting a good regression model. The study showed that fluid discharge characteristics such as temperature, velocity, pH, steam fraction and geometry of the well contribute about 56.71% to the thinning rate of the casing. The predicted thinning rate model also shows similar trending of the average thinning rate compared to the measured thinning rate for the first and second surveys of repeatedly measured wells.

1. INTRODUCTION

The objective of this study is to determine the significant factors and corrosive species that predominantly affect the thinning rate of production casing and to predict the thinning rate of the casing. This study is relevant in putting in place a systematic program for monitoring the casing conditions of a geothermal well. This study aims to provide an idea on the average thinning rate of the casing based on surface measured data of the well. The results of the study may also help to prioritize wells by programming caliper measurements for monitoring the rate of corrosion in the well casings. The study is limited to the production wells of Leyte geothermal production field (Figure 1) and concentrate only on the internal corrosion of the well.

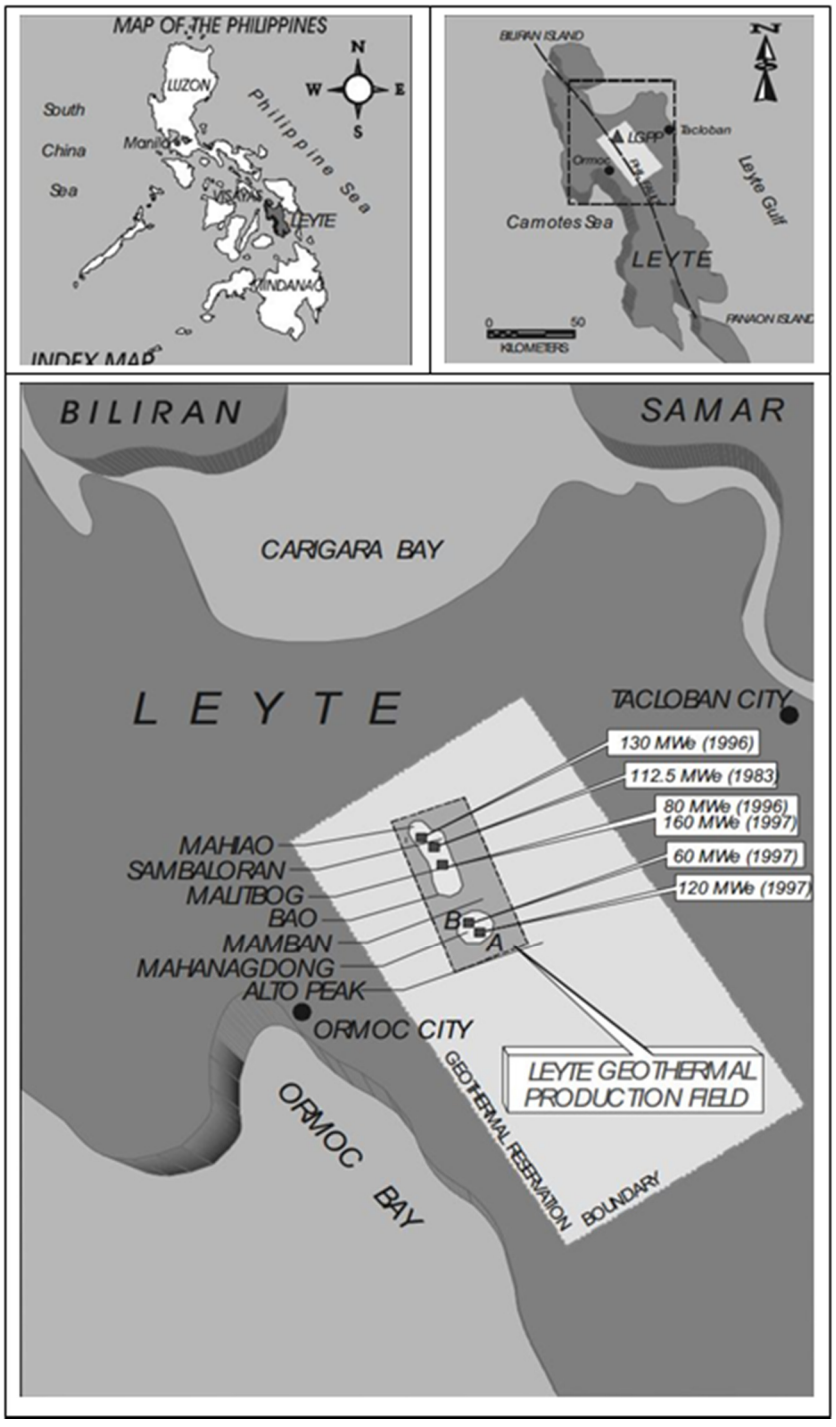

FIGURE 1: Location map of Leyte geothermal production field

After a geothermal production well is drilled and utilized to extract heat energy from a reservoir, certain problems occur and one of these problems is corrosion. Casing corrosion is one of the challenging technological problems in managing a geothermal production field. Scaling is another technological problem during geothermal utilization.

Geothermal fluids contain CO_2, H_2S, NH_3 and chloride ions that can cause the corrosion of metallic materials. The fluid characteristics change over time as heat extraction takes place. Thus, it is important to put in place a systematic procedure for monitoring the fluid chemistry of every geothermal well in operation.

The casings of geothermal wells, when exposed to the flow of geothermal brine flow, experience thinning. The thinning of the casing, primarily a result of material loss, compromises the casing's

integrity; this may eventually lead to casing breaks and casing collapse and, consequently, a reduction of well output. Casing breaks at shallow depths may cause steam to leak into the formation and within the pad. The steam leak within the overlap of the anchor casing and the production casing may lead to an underground blowout. The high risk involved with unreliable casing conditions requires systematic monitoring of the casing's integrity. This is for environmental and safety concerns and to ensure continuous geothermal well operation. The integrity of the casing is inspected by using downhole-logging tools such as caliper tools, electromagnetic tools, acoustic tools or video cameras; these tools are used to examine the condition of the casing.

The production casing in the geothermal fields of Cerro Prieto in Mexico experienced serious corrosion, both internal and external, after several years of production. To some extent, due to the extent of the corrosion of the casing, modifications, of both the grades of steel used and the thickness of the casing, were implemented in order to prolong usage of the well. In cases where the corrosion was extensive, the casings lasted only for two and a-half years after utilization (Ocampo-Diaz et al., 2005).

In the Krafla geothermal field, the carbon steel liner at the bottom of Well KJ-39 fractured and was severely corroded, caused by the aggressive nature of the fluid. Metallurgic examination of the liner indicated damage due to hydrogen embrittlement. Karlsdóttir and Thorbjörnsson (2012) found that abrupt changes in the environment had occurred at 1600 m, resulting in damage to the liner. The changes were a result of mixing two different transition systems: very hot dry steam containing H_2S, CO_2 and HCl, flowing upward; and a colder two-phase fluid. The mix resulted in a highly acidic fluid at the transition point.

A casing inspection caliper checked the condition of the casings of the production wells in the Leyte geothermal production field (Figure 1). In the Mahanagdong sector, the brine produced from the production wells has a very low pH. Hence, periodically, and using caliper surveys, the well casings were monitored for thinning. After several years of utilization, one of the production wells in the Mahanagdong area was plugged and then abandoned; the cause was severe corrosion.

The high-enthalpy single-phase steam-dominated wells of the Leyte geothermal production field were monitored using caliper measurements. There is severe corrosion in these wells because of the presence of a high quantity of suspended solids. The results of the caliper surveys served as a baseline for well utilization and intervention strategies in order to mitigate further deterioration of the casings.

The data, from the caliper surveys of production wells in Leyte geothermal production field, were used to study the thinning rate of the casings. The characteristics of the fluid discharge, such as fluid velocity, temperature, pH, and fluid chemistry concentration, were used to study the effects of the thinning rate on the casings.

2. CORROSION IN GEOTHERMAL WELLS

Corrosion is a damaging occurrence due to chemical or electrochemical action on the surrounding environment. It is detrimental to the appearance of metals and causes degradation of the equipment and material failure if kept unchecked. The corrosion process may assume several forms. On the overall surface of the metal, the reaction takes place slowly and reduces the thickness of the metal. In isolated areas, the corrosion may be localised. In some cases, the corrosion occurs on the weakest part of the metal where a difference in resistance to corrosive destruction is present. The differences in resistance in the metals are due to impurities and possible non-uniform treatment of the metal during manufacturing.

In a geothermal environment, the corrosion process depends upon the chemical composition of the geothermal fluid or brine. The geothermal brine has a wide range of composition, from strongly acidic

brine that corrodes most common alloys to the more usual neutral pH waters that may lay protective scales on the metal's surface (Elguedri, 1999).

In a high-temperature geothermal field, brine flashes inside the wellbore and changes from single-phase to two-phase due to the drop in pressure while the well is being flowed. Wahl (1977) discussed the effect of flashing on brine composition as the geothermal well produces steam. The flashing of the brine causes two main changes on the chemical concentration. First, evaporating some of the water in the brine achieves a higher concentration of the remaining components while the brine is flashed at a sufficiently low pressure. The ratio of the brine between after flashing and before flashing is dependent upon the weight fraction of the water flashed. Second is the effect of flashing on the chemistry of the brine. Flashing removes certain constituents such as carbon dioxide or hydrogen sulphide. As carbon dioxide is the dominant gas in the fluid mix, this will have the most significant effect on the chemistry of the fluid. The effect of CO_2 release is, in principle, the change in fluid pH. The next most significant is the reduction of dissolved CO_2 in the brine. When CO_2 dissolves in water, a small portion of it reacts chemically with H_2O to form carbonic acid. In water, carbonic acid dissociates rapidly to form H+ ion and HCO_2, so it affects carbonate equilibrium and pH values change as a result. The release of CO_2 from the solution will result in release of carbonate ions, causing the pH of the fluid to increase.

2.1 Corrosive species in geothermal brine

There are key chemical species that produce significant corrosion effects on metallic materials. Conover, et al. (1979) generalized the corrosive effects of these chemical species:

- *Hydrogen ion (H^+)* - Increasing the concentration of hydrogen (decrease in pH) will result in an increase in the rate of general corrosion for carbon steel, especially when fluid has a pH below 7. The metal in a fluid with pH higher than pH 7, (low concentration of hydrogen ion), forms a protective layer or film which minimizes the rate of corrosion. However, when the protective layer is broken, serious localized corrosion occurs which can cause pitting, crevice corrosion and stress corrosion cracking.
- *Chloride ion (Cl^-)* – The chloride ion causes the local breakdown of passive films that protect the metal from uniform corrosion, thus resulting in pitting, crevice corrosion, or stress corrosion cracking. An increase in chloride concentrations can also lead to an increase in uniform corrosion, but this is not as critical as the localized effect.
- *Hydrogen sulphide (H_2S)* – This corrosive specie is more severe for copper and nickel alloys. The effect of H_2S on iron-based materials is less predictable. It accelerates corrosion on the metal but, in some cases, it inhibits corrosion. High strength steels are often subject to sulphide stress cracking, which is a form of hydrogen embrittlement. The oxidation of hydrogen sulphide, in aerated geothermal process streams, increases the acidity of the streams. A low concentration of hydrogen sulphide may have serious detrimental effects, especially when oxygen is present.
- *Carbon dioxide (CO_2)* – In the acidic region, i.e. as in carbonic acid (H_2CO_3), it can accelerate the uniform corrosion of carbon steel. Carbon dioxide largely controls the pH of geothermal fluids and process streams. Carbonates and bicarbonates can display mild inhibitive effects.
- *Ammonia (NH_3)* – It can cause stress corrosion cracking of copper alloys and accelerate uniform corrosion in mild steels.
- *Sulphate (SO_4-)* – It plays a minor role in most geothermal fluids. However, in low chloride fluids, sulphate becomes the main aggressive anion; it rarely causes the same severity of the localized corrosion as the chloride ion.
- *Oxygen (O)* – Oxygen is present in low concentrations in geothermal brine. Inadvertent intrusion of even traces of this gas into geothermal brine has led to serious accelerated corrosion. The addition of minor quantities of oxygen to a geothermal system can increase the chances of severe localized corrosion of normally resistant alloys. The corrosion of carbon steels is sensitive to trace amounts of oxygen.

- *Transition metal ions* – Transition metal ions could also be included as a key species. Some oxidized forms of transition metals (Fe^{3+}, Cu^{2+} and others) are corrosive, but these ions are present in the lowest oxidized state in geothermal fluids. When transition metals are exposed to oxygen by aeration or mixing with water of different quality, oxygen can convert Fe^{2+} to Fe^{3+}, which is another reason for scrubbing oxygen from geothermal streams.

2.2 Types of corrosion encountered in geothermal systems

There are several types of corrosion attacks found in equipment used in a geothermal environment (Conover, et al., 1979). Some of the main modes of corrosion that occur in geothermal systems are as follows:

- *Uniform corrosion.* It is a general overall attack on the metal surface, often promoted by chloride, carbon dioxide, oxygen or ammonia.
- *Pitting.* This type of corrosive attack is localized which results in the development of small pits in the metal surface. Pits are associated with the breakage of the protective film on the surface of the metal. It is susceptible to increases in the chloride and hydrogen ion content of the fluid.
- *Crevice corrosion.* It is a localized type of corrosion, similar to pitting. This depends on geometry and forms in the crevices of the equipment.
- *Stress corrosion cracking.* This is a catastrophic type of failure promoted by a combination of tensile stress and the presence of chloride in the environment. The severity of the stress corrosion cracking increases with increasing temperature and in the presence of oxygen.
- *Sulphide stress cracking*. Similar to stress corrosion cracking, sulphide stress cracking is also a catastrophic type of failure that results from exposure under stress of susceptible materials to a hydrogen sulphide environment in an aqueous phase. Contrary to the stress corrosion cracking, sulphide stress cracking decreases in severity with increasing temperature, but low pH may greatly accelerate the failure.
- *Hydrogen blistering.* This is the rupture of a metallic material, caused when hydrogen is trapped in voids and accumulates at a sufficient pressure. This occurs in low strength alloy steel in aqueous solutions containing hydrogen sulphide. The material does not need to be stressed in order for hydrogen blistering to occur.
- *Intergranular corrosion.* This is a regional type of corrosion, which occurs around grain boundaries, or in the neighbour grains of metallic materials, with little or no attack on the bodies of the grains. The alloy disintegrates, loses its strength, or both.
- *Galvanic corrosion.* It occurs by electrical conduction of two different metals. The corrosion of a less noble material accelerates in this kind of corrosion. During material selection, the order of the galvanic series is a reference used for preventing galvanic corrosion.
- *Fatigue corrosion.* This is a premature fracture caused by fluctuating stress exposed in a corrosive environment. The fatigue corrosion limit is the largest stress applied under a given condition of stress, temperature, and corrosive environment, without causing the material to fail for a given number of cycles.
- *Erosion-corrosion*. It is the accelerated corrosion of one metal exposed to a corrosive fluid. This occurs when fluid flows faster than the critical velocity familiar to that metal. It is the abrasion of the metallic material by high velocity fluids on the hanging solid materials or particles. Metal exposed to this kind of corrosion does not form corrosive products on its surface.

2.3 Other factors affecting the rate of corrosion

Aside from the chemical species present in geothermal fluids that significantly affect the rate of corrosion of metal, there are other factors. Some of these other factors lead to types of erosion-corrosion,

where fluid contacts the metallic material and damages the protective film created from the initial corrosive reaction. These factors are related to hydrodynamic parameters such as the temperature, pH, fluid velocity, two-phase flow quality, geometry of the flow, and the pipe material component, which influence the erosion-corrosion mechanism (Petric and Ksiazek, 1997). Several studies and laboratory experiments have concentrated on the effect of environmental factors on the corrosion of materials.

Effect of pH. Low pH affects the uniform corrosion rate of low carbon and low alloyed steels. According to Ikeuchi et al. (1982), the corrosion rate of a material is: a) inversely proportionally to pH when the pH is in the range of 1 to 4 due to the active dissolution of materials; and b) is independent of pH when pH is in the range of 4 to 10. In flow accelerated corrosion, as the hot pH in the system become more acidic, the relative rate increases. The influence of pH on the erosion-corrosion is more serious than on corrosion alone.

Effect of velocity. According to Sanada et al. (1998), the rate of corrosion is independent of the flow rate when the flow rate ranges from 70 to 100 m/s. However, as the velocity increases, the corrosion rate increases. When the velocity approaches the velocity of sound, the material is damaged remarkably by cavitation-erosion (Ikeuchi et al., 1982).

Effect of temperature. Rates of corrosion are significantly dependent on temperature (Sanada et al., 1998). The effect of temperature is high for alloys that have intermediate performance. However, the pH still has the dominant effect on the rate of corrosion.

Effect of pipe geometry. Shape and size of a piping geometry has a significant impact on flow-accelerated corrosion. This factor affects localized velocities and turbulence within the pipe component. A complex geometry could increase the localized velocity in a given section by two to three times compared to the bulk velocity (Petric and Ksiazek, 1997).

Effect of fluid quality. In a two-phase flow, the fluid flows along the pipe wall. The temperature and pressure determine the amount of steam, according to the mass fraction of the quality of the water/steam mixture. The steam quality determines the distribution of the voids within the flow stream; that distribution, in turn, affects the mass transfer and rate of the flow-accelerated corrosion.

Effect of metal alloy content. The amount of alloy material present in the metal affects the stability and solubility of the oxide layer on the surface. Traces of molybdenum, copper and particularly chromium can have a significant impact on the rate of corrosion. The influence of pH on the rate of corrosion in a two-phase fluid shows the dependence of a material's composition on pH, as shown in the experiment by Sanada et al., (1995), wherein carbon and low alloy steels severely corroded at a pH less than 3.5.

3. GEOCHEMISTRY OF THE PHILIPPINE GEOTHERMAL FIELDS

The downhole pH and sulphur chemistry, as a function of boiling point temperatures, were determined for a number of wells from different fields; these could be linked to the sulphide mineralogy of rocks recovered from the acid Cl-SO_4 wells (Lichti et al., 1998). The produced fluids are classified as three types: low CL, high SO_4 with NA+K>Cl; high Cl, high SO_4 with CL>Na+K; and high Cl, high SO_4 with Na+K>Cl.

The Leyte geothermal production field in North Central Leyte is the largest geothermal area in the Philippines. It is a liquid-dominated high temperature geothermal field and its brine has neutral to low pH. The brine from the Mahanagdong sector of the Leyte geothermal production field has a pH ranging from 3 to 8, based on actual samples taken from the wells. It is inferred that the temperature of the aquifers in Mahanagdong ranges from 250 to 300°C; the aquifers have higher concentrations of H_2S and H_2 in the initial aquifer fluids (which are assumed to be purely liquid), than those at equilibrium with

the hydrothermal mineral assemblage (Angcoy, 2010). The Mahanagdong field discharges low pH fluid with high salinity and has either high or low sulphate concentrations. The reservoir fluids with high sulphate acidic fluids have a high concentration of the HSO_4 species that dissociates at a lower temperature, resulting in an acidic fluid discharge at the wellhead (Cabahug and Angcoy, 2013).

4. RESEARCH METHODOLOGY

4.1 Data preparation

The data obtained from the casing inspection caliper runs, conducted on geothermal wells of Leyte geothermal production field, were used for statistical analysis. The thinning rate (TR) of the casings was calculated using Equation 1, based on the measured pit depth, obtained from the multifinger arm caliper tool. Table 1 summarizes the caliper survey conducted on the two-phase and dry wells of the Leyte geothermal production field.

$$TR = \frac{pitdepth\ (mm)}{time\ (years)} \tag{1}$$

TABLE 1: Summary of the caliper survey conducted on the two-phase and dry wells of Leyte geothermal production field

	Two-phase wells	**Dry wells**
No. of wells surveyed	19	16
Length of cased hole	739 - 1948 m	475 - 1657 m
Casing diameter	177.80 - 339.73 mm	244.48 - 339.73 mm
Total mass flow	5-55 kg/s	3 - 25.2 kg/s
Enthalpy	1056 -2536 kJ/kg	~ 2700kJ/kg

The multi-finger caliper used is the memory type 30-finger arms caliper shown in Figure 2. Its 30-feeler arms record the radii of the casing and provide a complete representation of the well casing condition. The mechanical caliper is among the simplest and most accurate tools available on the market for measuring the internal diameter of the casing. It is useful for analysing internal corrosion damage, scale build-up, collapsed and parted casing breaks. The tool consists of a centralizer to put the tool in-centre inside the casing, and a caliper finger arm, which reaches out to the inside of the casing wall. Caliper finger arms are made of tungsten carbide, tipped for wear. A mechanical tripper opens the memory-type caliper tool. From the 30 radii recorded, the maximum measured inner diameter of the casing was used to represent the minimum thickness of the casing at depth.

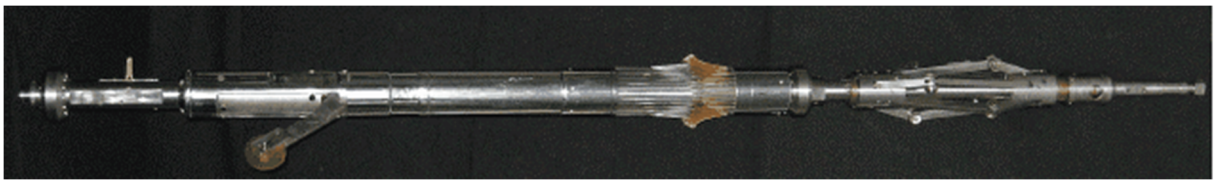

FIGURE 2: Photo of a 30-arm Multifinger caliper tool

The downhole temperature, fluid velocity, and steam fraction were obtained by wellbore simulation, using the software package, HOLA. HOLA reproduces the measured flowing temperature and pressure profiles in flowing wells and determines the relative contribution of each feedzone for a given discharge condition (Björnsson et al., 1993). The simulator can handle both single and two phase flows in vertical pipes and calculates the flowing temperature and pressure profiles in a well. It solves numerically the differential equations that describe the steady-state energy, mass and momentum flow in a vertical pipe.

The flow within the well was assumed to be in steady state at all times, but the reservoir pressure was allowed to vary with time. Top-down simulations were conducted where the downhole well conditions were simulated based on given wellhead conditions, such as mass flowrates and enthalpy values. There was no comparison made between the simulated temperature and pressure profiles and the measured flowing temperature and pressure profiles of all the wells, because flowing surveys were not available for all of them. To simplify the simulation process and since the cased hole section is the main point of interest, it was assumed that the depth of the feedzone was at the production casing shoe with the properties of the flow discharge. Table 2 shows the well discharge data used at wellhead conditions, while Table 3 summarizes the simulated downhole results given by HOLA.

TABLE 2: Fluid discharge data of two-phase and dry wells studied for predicting the thinning rate of the casing

Well name	Date sampled	WHP	MF	H	Well name	Date sampled	WHP	MF	H
Well 1	6-May-12	1.10	48.5	1736	Well 20	30-Oct-11	1.1	18.4	2779
Well 2	11-May-11	1.10	4.7	2435	Well 21	4-May-11	1.0	7.5	2777
Well 3	4-Nov-10	1.10	36.8	1687	Well 22	15-Sep-11	1.0	6.8	2777
Well 4	8-Dec-11	1.10	28.0	1611	Well 23	23-Jul-11	1.0	16.7	2777
Well 5	27-Nov-10	1.10	24.0	1632	Well 24	26-Jan-12	1.0	3.0	2777
Well 6	22-Aug-12	1.1	55.2	1056	Well 25	28-Apr-11	1.5	19.1	2788
Well 7	3-Apr-12	1.1	40.6	1085	Well 26	2-Sep-11	1.8	20.0	2796
Well 8	30-Oct-10	1.1	50.6	1315	Well 27	13-Sep-11	1.23	25.2	2787
Well 9	11-Nov-10	1.1	54.4	1194	Well 28	12-Aug-11	1.02	8.5	2779
Well 10	19-Jun-09	1.1	39.1	1178	Well 29	10-Mar-11	1.1	9.9	2781
Well 11	4-Nov-12	1.3	32.2	1659	Well 30	9-Aug-12	*1.4*	13.6	2787
Well 12	26-Feb-11	1.22	29.1	1283	Well 31	4-Sep-10	1.4	23.9	2549
Well 13	13-Sep-11	1.25	42.4	2476	Well 32	26-Jan-13	1.5	5.3	2778
Well 14	26-Nov-12	1.11	30.04	1165	Well 33	7-Dec-11	1.5	19.6	2697
Well 15	20-May-11	1.8	20.9	1482	Well 34	13-Oct-10	1.45	14.2	2789
Well 16	22-Dec-12	1.35	18.86	2413	Well 35	11-Jan-12	1.2	6.5	2789
Well 17	11-Nov-12	1.7	26.4	1325					
Well 18	11-Aug-12	1.42-1.55	25.1	2536					
Well 19	23-Jul-12	1.2	10.6	2312					

WHP: Wellhead pressure; **MF**: Mass Flow; **H**: Enthalpy

TABLE 3: Summary of simulated downhole data using software HOLA

Type	No of wells	Range of temperature (°C)	Range of fluid velocity (m/s)
Two-phase well	19	188 – 288	3.5 - 110
Dry well	16	184 – 236	13 - 98

The software WATCH simulated the fluid chemistry concentrations of pH, Cl, SO_4, H_2S, CO_2 and H_2 in the geothermal brine at downhole conditions. The Icelandic Water Chemistry group presented the software WATCH as a chemical speciation program for UNU fellows in 1993. It interprets the chemical composition of geothermal fluids. The program reads the chemical analyses of water, gas and steam condensate samples, collected at the surface, and computes the chemical composition of downhole or aquifer fluids. This includes the pH, aqueous speciation, partial pressures of gases, redox potentials, and activity products for mineral dissolution reactions (Arason et al., 2003). Figures 3 and 4 shows the water and gas chemistry data of each well surveyed, while Table 4 summarizes the simulated downhole results given by WATCH.

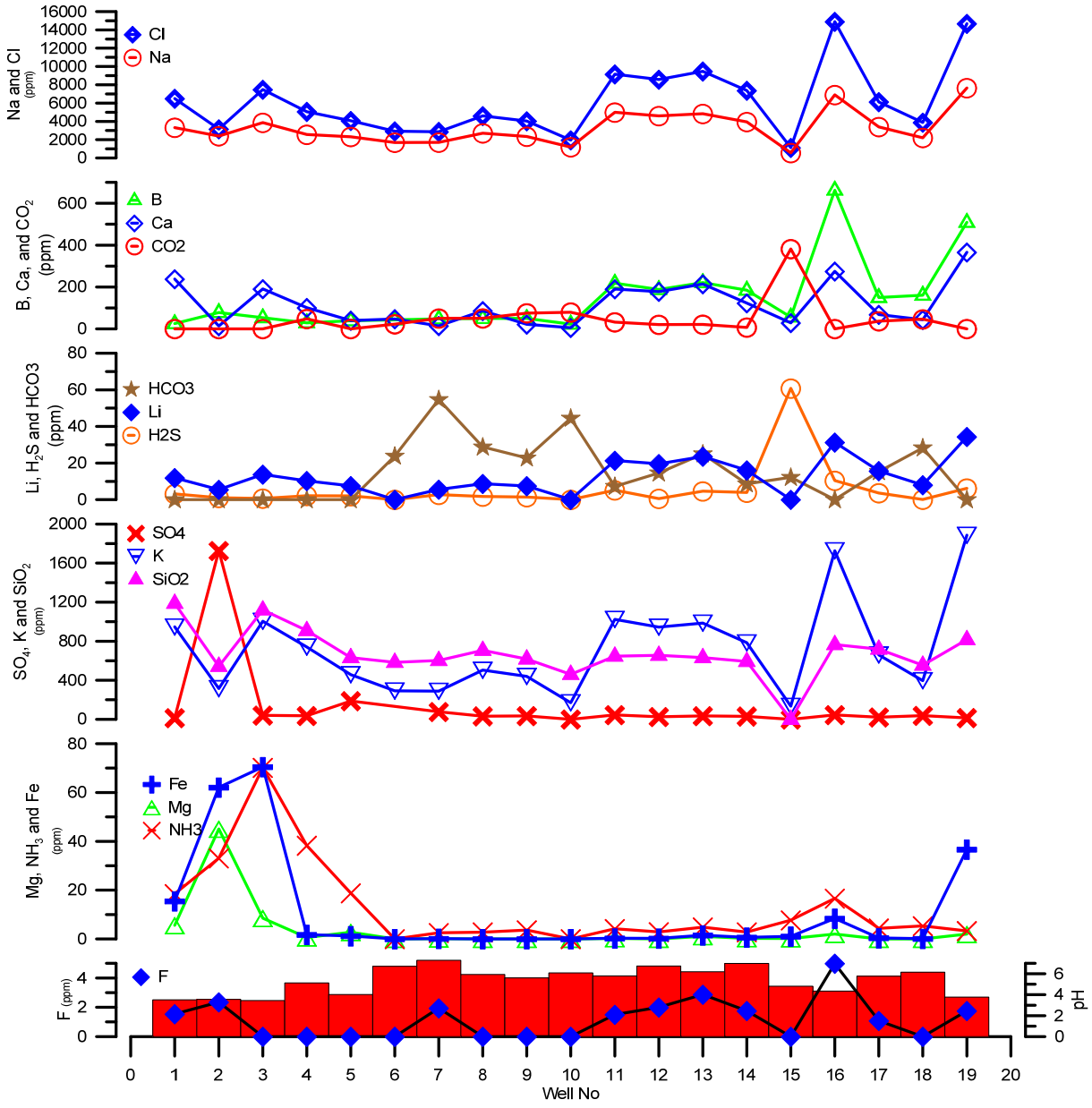

FIGURE 3: Sampled water chemistry data of two-phase wells

TABLE 4: Summary of simulated concentrations of corrosive species using software WATCH

Range of simulated downhole chemistry of the well studied							
Cl_w (ppm)	**SO_{4w} (ppm)**	**CO_{2w}(ppm)**	**H_2S_w (ppm)**	**CO_{2g} (ppm)**	**H_2S_g (ppm)**	**H_{2g} (ppm)**	**Range of fluid pH**
970 -15097	0 - 1701	11 - 1205	Feb-54	3578 – 56071	176 - 1534	0.1 - 7.13	3.6 - 6.9

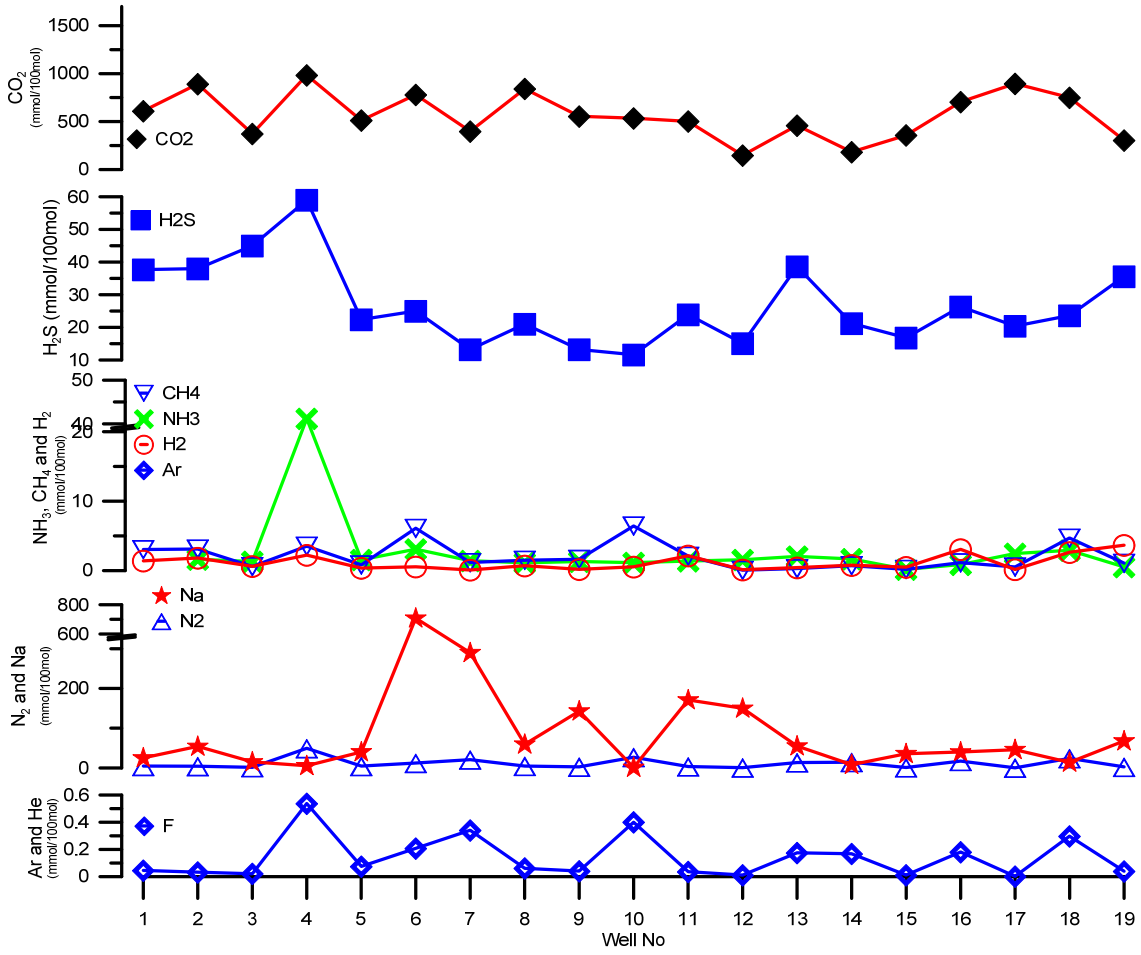

FIGURE 4: Sampled gas chemistry data of two-phase wells

Table 5 summarizes the total suspended solids (TSS) data, measured at the surface. This parameter was not included in the simulation. It was assumed that the TSS concentration at the surface was constant throughout the cased hole. The simulation of TSS is very complex because, aside from the particles coming from the open hole section, the eroded particles from the casing could be contributing to the measured TSS at the surface.

TABLE 5: Measured total suspended solids (ppm) in dry wells

Well 20	Well 21	Well 22	Well 23	Well 24	Well 25	Well 26	Well 27	Well 28	Well 29	Well 30	Well 31	Well 32	Well 33	Well 34	Well 35
10.5	2.5	2.96	29.6	2.5	2.5	6.7	2.5	2.5	2.5	9.6	45.4	2.5	2.72	9.9	2.5

The effect of well geometry on the impact of flow particles as a function of well inclination θ was obtained using the equation given by Finnie et al. (1992). The well inclination of the well was taken from the deviation survey of the well.

For $\theta \leq 18.5^{o}$:

$$f(\theta) = (\sin 2\theta - 3sin^{2}\theta) \tag{2}$$

And for higher inclinations, $\theta > 18.5^{o}$:

$$f(\theta) = \frac{cos^{2}\theta}{3} \tag{3}$$

4.2 Development of a corrosion model

The thinning rate of the casing can be expressed as a function of the factors affecting the rate of corrosion according to the following:

$$TR = f\left(T, V_s, pH, X, f(\theta)\right) \tag{4}$$

$$TR = f\left(Cl_w, H_2S_w, SO_{4w}, CO_{2w}, H_{2g,} H_2S_g, CO_{2g}\right) \tag{5}$$

where TR = Average thinning rate of casing joint (mm/year);
T = Simulated downhole temperature (°C);
V_s = Simulated fluid velocity (m/s);
pH = Fluid pH;
X = Steam fraction;
$f(\theta)$ = Effect of well inclination;
TSS = Total suspended solids (ppm);
Cl_w = Chloride concentration in water (ppm);
H_2S_w = Hydrogen sulphide in water (ppm);
CO_{2w} = Dissolved Carbon dioxide in water (ppm);
SO_{4w} = Sulphate in water (ppm);
H_2S_g = Hydrogen sulphide gas (ppm);
CO_{2g} = Carbon dioxide gas(ppm);
$H_{2g,}$ = Hydrogen gas (ppm).

To model the effect of the above-mentioned factors on the thinning rate of the casing, a linear regression model was developed. Regression analysis is a statistical process used for estimating the relationships between variables. Regression analysis seeks to determine the causal effect of one variable upon another. The regression analysis helps in understanding how the typical values of dependent variables change when any one of the independent variables is varied, and the rest of the independent variables are kept constant.

The regression equation used for predicting the impact of the factors affecting the casing's thinning rate was based on the mathematical model for flow-accelerated corrosion, in which the affecting factors are interrelated, as shown in Equation 6 (Petric and Ksiazek, 1997).

$$WR = F(MT) * F(G) * F(X) * F(pH) * F(O2) * F(T) * F(AC) \tag{6}$$

where WR = Wear rate
$F(MT)$ = Factor for mass transfer effect
$F(G)$ = Factor for geometry effect
$F(X)$ = Factor for void fraction (steam quality)
$F(pH)$ = Factor for pH effect
$F(O_2)$ = Factor for Oxygen effect
$F(T)$ = Factor for temperature effect
$F(AC)$ = Factor for alloy content effect

Logarithmic transformation of data was used to set up the multiplicative factors to form a linear equation. This was done by taking the logarithmic form of both sides of Equation 7 and the identity of the logarithm of (A * B) which is log A + log B. The multiplicative function can be expressed in a linear equation, as shown in Equation 8, which can be used for linear regression as shown in Equation 9:

$$TR = A * T * V_s * pH * X * f(\theta) \tag{7}$$

$$Ln(TR) = Ln(A * T * V_s * pH * X * f(\theta)) \tag{8}$$

$$Ln(TR) = Ln(A) + Ln(T) + Ln(V_s) + Ln(pH) + Ln(X) + Ln(f(\theta)) \tag{9}$$

Different cases of regression equations were used. For the corrosive species, an additive form and multiplicative forms were used. The additive form is the simplest model form for a regression. The multiplicative form for a regression for the corrosive species was included as a check to see if the interrelated model of the corrosion species would provide a better model for predicting the thinning rate of the casing. The list of cases for the regression analysis, the corrosive species, and the relevant factors included in the regression are summarized in Table 6.

TABLE 6: Regression equation for two-phase wells in predicting the thinning rate of the casing using the affecting factors

Case	Regression model
1	$Ln(TR) = \beta_{10} + \beta_{11}Ln(T) + \beta_{12}Ln(V_s) + \beta_{13}Ln(pH)$
2	$Ln(TR) = \beta_{20} + \beta_{21}Ln(T) + \beta_{22}Ln(V_s) + \beta_{23}Ln(pH) + \beta_{24}Ln(f(\theta))$
3	$Ln(TR) = \beta_{30} + \beta_{31}Ln(T) + \beta_{32}Ln(V_s) + \beta_{33}Ln(pH) + \beta_{34}Ln(X) + \beta_{35}Ln(f(\theta))$
4	$TR = \beta_{40} + \beta_{41}Cl_w + \beta_{42}H_2S_w + \beta_{43}SO_{4w} + \beta_{44}CO_{2w} + \beta_{45}H_{2g} + \beta_{46}H_2S_g + \beta_{47}CO_{2g}$
5	$Ln(TR) = \beta_{50} + \beta_{51}Ln(Cl_w) + \beta_{52}Ln(H_2S_w) + \beta_{53}Ln(SO_{4w}) + \beta_{54}Ln(CO_{2w}) + \beta_{55}Ln(H_{2g}) + \beta_{56}Ln(H_2S_g) + \beta_{57}Ln(CO_{2g})$
6	$Ln(TR) = \beta_{60} + \beta_{61}Ln(V_s) + \beta_{62}Ln(f(\theta) + \beta_{63}Ln(T) + \beta_{64}Ln(TSS)$

where β_{i0} and β_{ik} are the normal and slope coefficients due to the affecting factors, and corrosive species $(T, V_s, pH, X, f(\theta), Cl_w, H_2S_w, SO_{4w}, CO_{2w}, H_{2g}, H_2S_g, CO_{2g})$. The regression model of cases 1 to 6 can be written as a single matrix equation, as shown in Equation 10:

$$y_{(n+1)} = x_{(nk+1)}\beta_{(k+1)} \tag{10}$$

where $x = (T, V_s, pH, X, f(\theta), Cl_w, H_2S_w, SO_{4w}, CO_{2w}, H_{2g}, H_2S_g, CO_{2g})$, and $y = (TR_1, TR_2, .TR_{1n})$, which is a vector of the measured thinning rate at different levels of the affecting parameters (x variables).

Affected parameters in the thinning rate can be shown in matrix form *X*,

$$x = \begin{bmatrix} 1 & x_{11} & \dots & x_{1k} \\ 1 & x_{21} & \dots & x_{2k} \\ 1 & x_{n1} & \dots & x_{nk} \end{bmatrix} \tag{11}$$

where $\beta = (\beta_0, \beta_1, \beta_2, \dots, \beta_k)'$ values contain the regression coefficients due to the factors affecting the thinning rate. The residual sum of squares is solved by including an error factor (e) in Equation 10.

The transformation equations leading to a normalized form of the equation are given in Equation 14:

$$\underset{(k+1\ \ xk+1)}{x'x\beta} = \underset{(k+1\ \ x1)}{xy'} \tag{12}$$

$$x'x = \begin{bmatrix} n & \sum x_{i1} & \sum x_{i2} & \dots & \sum x_{ik} \\ \sum x_{i1} & \sum x_{i1}^2 & \sum x_{i1}x_{i2} & \dots & \sum x_{i1}x_{ik} \\ \sum x_{i2} & \sum x_{i1}x_{i2} & \sum x_{i1}^2 & \dots & \sum x_{i2}x_{ik} \\ \vdots & \vdots & \vdots & \vdots & \vdots \\ \sum x_{ik} & \sum x_{i1}x_{ik} & \sum x \;\; x & \dots & \sum x_{i1}^2 \end{bmatrix} \tag{13}$$

$$xy' = \begin{bmatrix} \sum y_i \\ \sum x_{i1}y_i \\ \sum x_{i2}y_i \\ \vdots \\ \sum x_{ik}y_i \end{bmatrix} \tag{14}$$

The solution of the normalized Equation 12 provides a solution of the independent coefficients of the operating parameters and is given in Equation 15:

$$\beta = \left(x'x\right)^{-1}xy' \tag{15}$$

The multiple regression and the analysis of variance (ANOVA) test were performed at a 95% confidence level in order to examine the combined effects of temperature, fluid velocity, fluid pH, well geometry, steam fraction, and corrosive species such as chloride, sulphate, hydrogen, carbon dioxide and hydrogen sulphide on the thinning rate of the geothermal well casing.

4.3 Selection of a good model

In selecting a good model for predicting the thinning rate casing, two criteria are used. The first criterion is use of the adjusted coefficient of determination (R_a^2) and the second is the mean absolute percentage error.

The adjusted coefficient of determination, (R_a^2), is a variation of R^2, which is proportional to the variation of the response variable.

$$R_a^2 = \left(\frac{MS_{Tot} - MS_{error}}{MS_{Tot}}\right) \tag{16}$$

where MS = Mean of squares.

This kind of variation or R^2 includes a penalty for unnecessarily explanatory variables. It measures the proportion of the observed spread in the responses explained by the model. The higher value of adjusted R^2 illustrates a good correlation.

Another criterion used in selecting the model is the mean absolute percentage error (MAPE). It is a measure of the accuracy of a method for constructing fitted values in statistics, specifically for estimation. MAPE is expressed as a percentage as shown in Equation 17. The model with lower MAPE is a good prediction model.

$$MAPE = \frac{1}{n}\sum_{i}^{n}\left|\frac{Actual_i - Predicted_i}{Actual_i}\right| R_a^2 = \left(\frac{MS_{Tot} - MS_{error}}{MS_{Tot}}\right) \tag{17}$$

5. RESULTS AND DISCUSSION

The correlation results of the thinning rate in the casing as a dependent variable, and the factors affecting it ($T, V_S, pH, X, f(\theta),$), are summarized in Table 7.

TABLE 7: Correlation results of the thinning rate in the casing

Case model	Multiple R	R^2	Adjusted R^2	Standard error	Observation
1	0.7247	0.5252	0.5240	0.8870	1188
2	0.7467	0.5576	0.5561	0.8566	1188
3	0.7543	0.5689	0.5671	0.8459	1188
4	0.7415	0.5499	0.5472	0.1910	1188
5	0.6627	0.4391	0.4358	0.9657	1188
6	0.4101	0.1682	0.1634	0.9484	700

The coefficient of determination R^2 ranges from 0.5252 to 0.5689 for cases 1 to 3, while the adjusted R^2 ranges from 0.5240 to 0.5671. This implies that a combination of factors such as temperature, fluid velocity and fluid pH, contributes 52.40% to the thinning rate of the casing of geothermal well. On the other hand, a combination of the temperature, fluid velocity, steam fraction, well geometry and fluid pH factors contributes 56.71% to the thinning rate. For the regression of the corrosive species found in the two-phase wells, 54.72% was the additive term of the species' contribution to the thinning rate of the casing. The adjusted R^2 of the regression for dry wells shows that 16.34% of the thinning rate comes from the effects of velocity, temperature, well geometry and total suspended solids, which is a very low correlation on the thinning rate of the casing.

The low value of coefficient determination could be the result of the effects of other factors, such as the condition of the casing used in the geothermal well. It is possible that the casing had pitting inside before it was installed in the borehole. Well stimulation conducted on the geothermal well, like a drilling work-over, for example by the drill bit as it is run in hole inside the well during mechanical clearing operations, could significantly affect the condition of the casing. During clearing operations, a casing joint section located at a high inclination could be much affected by the drill pipe.

Higher residuals were observed for cases 1 to 3, 5 and 6, mainly because they were logarithmically transformed, when compared to case 4. Since the coefficient of determination of the resulted regression is low, the residual of the regression is high. In addition, since the data is log-transformed, any error or change in the value of an outcome variable is presented as a percentage of the value. The percentage of change was multiplied for each term of the variable; this makes the residual value of the model high.

Table 8 shows ANOVA results of the thinning rate of the casing and all of the relevant factors. All of the regression cases were highly significant to the thinning rate of the casing. Intuitively, the thinning rate can be determined using the factors used. However, the adjusted R^2 (please refer to Table 7) values are still low, indicating that the model needs further improvement; the model can be used as a good prediction model.

The P value of the variables shows that the coefficient of the factors for cases 1 to 6 has values lower than 0.05, using a 95% confidence interval for all variables as shown in Table 9. This shows that the test is statistically significant. Case 4 of the regression model shows that the corrosive species CO_{2w} and H_2S_w are not significant in the additive terms of the regression model of the thinning rate. The case 4 regression model was reduced to the form of Equation 18, and the result of the regression is shown in Table 10.

TABLE 8: Summary of ANOVA for the casing thinning rate and affecting factors

Case model		df	SS	MS	F	Significance
1	Regression	3	1030.3319	343.4440	436.4842	6.57×10^{-191}
	Residual	1184	931.6205	0.7868		
	Total	1187	1961.9524			
2	Regression	4	1093.9418	273.4854	372.7296	1.08×10^{-207}
	Residual	1183	868.0106	0.7337		
	Total	1187	1961.9524			
3	Regression	5	1116.2291	223.2458	312.0128	4.80×10^{-213}
	Residual	1182	845.7234	0.7155		
	Total	1187	1961.9524			
4	Regression	7	52.5885	7.5126	205.9238	1.70×10^{-199}
	Residual	1180	43.0495	0.0365		
	Total	1187	95.6380			
5	Regression	7	861.5407	123.0772	131.9789	2.23×10^{-143}
	Residual	1180	1100.4117	0.9326		
	Total	1187	1961.9524			
6	Regression	4	126.3930	31.5982	35.1316	9.61×10^{-27}
	Residual	695	625.1012	0.8994		
	Total	699	751.4942			

Case 4 (reduced form):

$$TR = \beta_{40} + \beta_{41}Cl_w + \beta_{42}SO_{4w} + \beta_{43}H_{2g} + \beta_{44}H_2S_g + \beta_{45}CO_{2g} \quad (18)$$

The parameter estimates of the variables shown in Tables 9 and 10 were analysed. Cases 1 to 3 of the factors affecting the thinning rate of the two-phase wells such as temperature, fluid velocity and fluid pH have negative coefficients, indicating a decreased effect on the thinning rate as the value of variables is increased. The increase in the steam fraction and well inclination corresponds to an increase in the thinning rate of the casing, as interpreted from the coefficient of the parameter estimates.

The plot of the average thinning rate of the wells, vis-a-vis the temperature at the wellhead, is shown in Figure 5. The plot shows a decreasing trend in the average thinning rate of the casing as the temperature of the wells at the surface increases for the 19 two-phase wells that were included in the study. The trend of the maximum thinning rate of the two-phase wells against simulated temperature at depth showed no apparent change in the trend between the temperature ranges. However, when only two-phase wells with higher pH ranging from 5 to 6 were considered, a decreasing trend was found in the thinning rate of the well with increasing temperature, shown in Figure 6. It is possible that within the well studied, as the fluids were boiled, the pH of the fluid decreased and moved to the surface. The temperature of the fluid decreases due to pressure drop as the fluid flows to the surface. The resultant decrease in pH fluids corrodes the casing of the well. This was observed by Lichti et al. (1998): in the potential-pH Pourbaix diagram of Mahanagdong well MG-9D, as the temperature decreased in the two-phase flow, small changes in

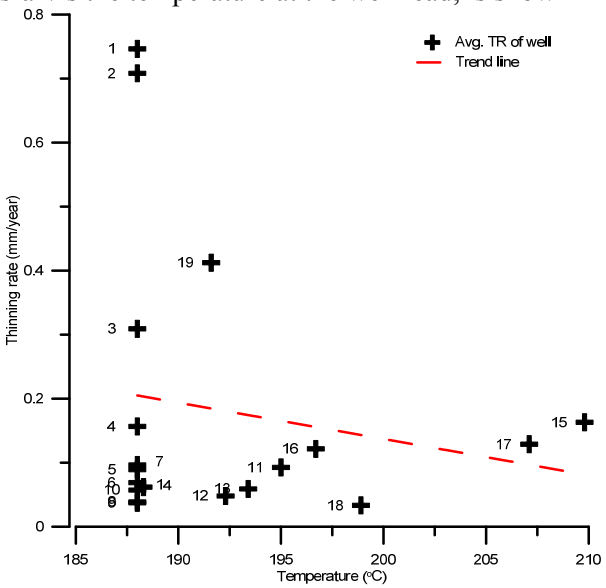

FIGURE 5: Plot of average thinning rate of two-phase wells against temperature at the wellhead

TABLE 9: Summary of parameter estimates

Case model	Variables		Coefficients	Standard error	t Stat	P-value
1	Intercept	β_{10}	29.4158	1.7118	17.1841	2.92×10^{-59}
	$Ln(T)$	β_{11}	-3.6181	0.2898	-12.4852	1.07×10^{-33}
	$Ln(V_s)$	β_{12}	-0.7349	0.0433	-16.9838	4.59×10^{-58}
	$Ln(pH)$	β_{13}	-5.9338	0.1658	-35.7958	8.72×10^{-191}
2	Intercept	β_{20}	30.8487	1.6602	18.5816	7.98×10^{-68}
	$Ln(T)$	β_{21}	-4.1648	0.2859	-14.5655	2.50×10^{-44}
	$Ln(V_s)$	β_{22}	-0.5784	0.0450	-12.8427	1.95×10^{-35}
	$Ln(pH)$	β_{23}	-5.1166	0.1826	-28.0276	5.59×10^{-133}
	$Ln(f(\theta)$	β_{24}	0.0720	0.0077	9.3109	5.97×10^{-20}
3	Intercept	β_{30}	23.4251	2.1111	11.0959	2.77×10^{-27}
	$Ln(T)$	β_{31}	-3.0741	0.3434	-8.9522	1.32×10^{-18}
	$Ln(V_s)$	β_{32}	-0.7261	0.0518	-14.0303	1.77×10^{-41}
	$Ln(pH)$	β_{33}	-4.5885	0.2036	-22.5374	7.44×10^{-94}
	$Ln(X)$	β_{34}	0.3005	0.0538	5.5811	2.96×10^{-08}
	$Ln(f(\theta)$	β_{35}	0.0529	0.0084	6.3153	3.81×10^{-10}
4	Intercept	β_{40}	2.61×10^{-02}	0.0241	1.0815	2.80×10^{-01}
	Cl_w	β_{41}	-1.09×10^{-05}	0.0000	-5.0462	5.22×10^{-07}
	H_2S_w	β_{42}	-3.18×10^{-03}	0.0019	-1.6717	9.49×10^{-02}
	SO_{4w}	β_{43}	2.80×10^{-04}	0.0000	20.1761	5.22×10^{-78}
	CO_{2w}	β_{44}	1.11×10^{-05}	0.0001	0.0951	9.24×10^{-01}
	H_{2g}	β_{45}	4.86×10^{-02}	0.0058	8.4308	9.89×10^{-17}
	H_2S_g	β_{46}	3.73×10^{-04}	0.0000	7.8152	1.21×10^{-14}
	CO_{2g}	β_{47}	-4.94×10^{-06}	0.0000	-3.1630	1.60×10^{-03}
5	Intercept	β_{50}	-4.4051	1.4990	-2.9387	3.36×10^{-03}
	$Ln(Cl_w)$	β_{51}	-0.7249	0.0555	-13.0570	1.71×10^{-36}
	$Ln(H_2S_w)$	β_{52}	0.9019	0.2729	3.3046	9.80×10^{-04}
	$Ln(SO_{4w})$	β_{53}	0.0653	0.0087	7.4773	1.48×10^{-13}
	$Ln(CO_{2w})$	β_{54}	-1.3214	0.2644	-4.9968	6.71×10^{-07}
	$Ln(H_{2g})$	β_{55}	0.4364	0.0419	10.4157	2.30×10^{-24}
	$Ln(H_2S_g)$	β_{56}	0.6935	0.2239	3.0976	2.00×10^{-03}
	$Ln(CO_{2g})$	β_{57}	0.7771	0.2765	2.8102	5.03×10^{-03}
6	Intercept	β_{60}	-19.8154	3.7784	-5.2444	2.08×10^{-07}
	$Ln(V_s)$	β_{61}	-0.2237	0.0884	-2.5311	1.16×10^{-02}
	$Ln(f(\theta)$	β_{62}	0.0718	0.0137	5.2574	1.95×10^{-07}
	$Ln(T)$	β_{63}	3.5387	0.7192	4.9203	1.08×10^{-06}
	$Ln(TSS)$	β_{64}	0.1368	0.0445	3.0745	2.19×10^{-03}

the stability of iron sulphide were observed. However, due to a continuing decrease in pH, the corrosion reaction moved from the limits of FeS into Fe^{++}, which is free of corrosion. This signifies that the pH of the fluid predominantly controls the thinning rate of the casing and is in agreement with the experimental results of Sanada et al. (1998); thus, the ph of the fluid predominantly controls the rate of corrosion.

The thinning rate of the casing is also higher in the low velocity range, as shown in Figure 7. The velocity of the fluid at downhole increases as the fluid phase changes from single to two-phase, as induced by boiling. The observed trend of a higher thinning rate at lower fluid velocity implies that thinning of the casing occurs at the velocity where the fluid is in a liquid phase condition. Slow velocity of the fluid results in longer residency time; this gives more time for thinning reactions at the surface of the casing. Most of the wells with higher thinning rates were wells with low pH fluid (Wells 1, 2, 3, 19, 16 and 15).

TABLE 10: Regression analysis, ANOVA and parameter estimate of reduced form of case 4

Case model	Multiple R	R^2	Adjusted R^2	Standard error	Observation
4 (reduced form)	0.7401	0.5478	0.5459	0.1913	1188

Case model		df	SS	MS	F	Significance
4 (reduced form)	Regression	5	52.3903	10.4781	286.3757	8.82E-201
	Residual	1182	43.2477	0.0366		
	Total	1187	95.6380			

Case model	Variables		Coefficients	Standard error	t Stat	P-value
4 (reduced form)	Intercept	β_{40}	0.04718	0.02057	2.29370	2.20E-02
	Cl_w	β_{41}	-0.00001	0.00000	-4.89714	1.11E-06
	SO_{4w}	β_{42}	0.00030	0.00001	26.33232	1.26E-120
	H_{2g}	β_{43}	0.05119	0.00566	9.04524	5.98E-19
	H_2S_g	β_{44}	0.00030	0.00002	12.23086	1.78E-32
	CO_{2g}	β_{45}	-0.00001	0.00000	-7.10980	2.01E-12

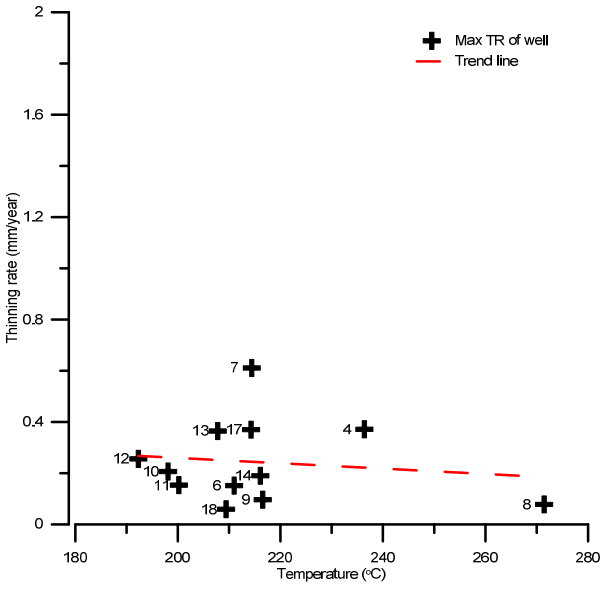

FIGURE 6: Maximum thinning rate of two-phase wells with pH > 5 plotted against its corresponding downhole temperature

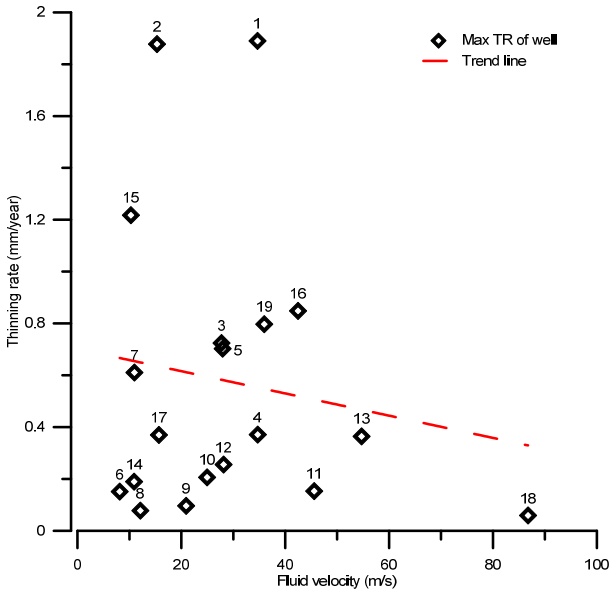

FIGURE 7: Plot of maximum thinning rates of wells with corresponding fluid velocity

The results of the regression for the two-phase wells were analysed. The parameter estimates of fluid pH showed a trend of a decreasing rate of corrosion as the pH of the fluid increased. This is in agreement with the findings from the corrosion study by Sanada et al. (1998) which said that a higher corrosion rate occurs at low pH. The plot of the maximum thinning rate with corresponding pH with depth is shown in Figure 8.

The plot of the maximum thinning of the casing with its corresponding steam fraction illustrates a trend of an increasing thinning rate in relation to the steam fraction, as shown in Figure 9. The result of the regression of the steam fraction shows that the thinning rate of the casing increases with increased steam fractions. The plot demonstrates that the maximum thinning rates were found in wells with low pH fluid. The flashing of the geothermal brine changed the concentration of the dissolved gasses and these resulted in a decrease in pH in the wells studied.

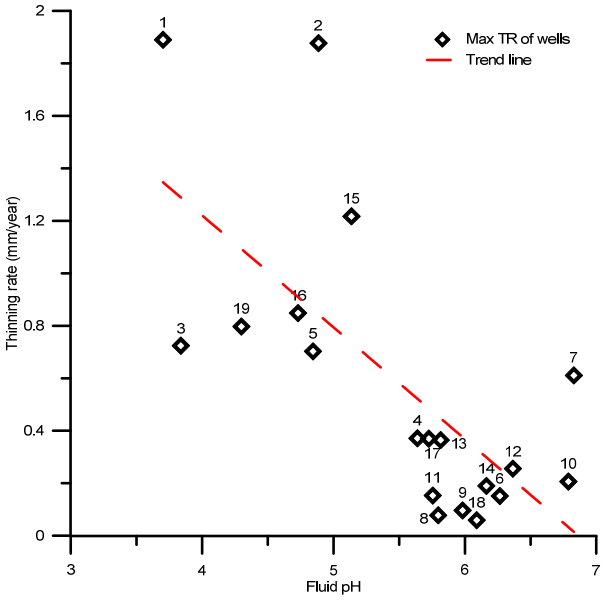

FIGURE 8: Plot of maximum thinning rate of well with its corresponding fluid pH

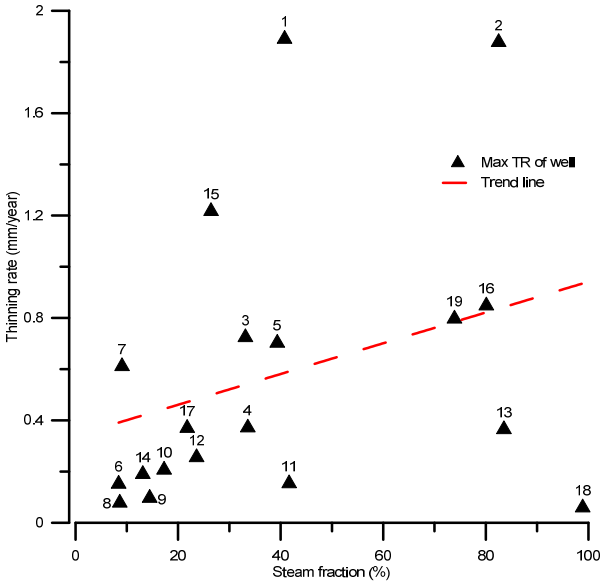

FIGURE 9: Plot of maximum thinning rate with its corresponding steam fraction

Based on the regression analysis, the deviated well geometry shows an increased effect in the thinning rate. However, the contribution of this factor to the thinning rate is very low when compared to other factors. A deviated well geometry will cause more turbulence in fluid flow. The rate of corrosion is much higher for a turbulent flow having a low pH concentration (Sanada et al., 1998).

Parameter estimates of the corrosive species of the reduced form of case 4 shows that for the studied wells, species of H_2S gas and H_{2g} significantly contribute to the thinning rate of the casing. Figure 10 illustrates a trend of an increasing thinning rate with respect to an increase in H_2S gas concentration. The casings used in most the geothermal wells are carbon steel K55. This type of casing has a small percentage of copper and nickel; when hydrogen sulphides are present, the corrosion is severe.

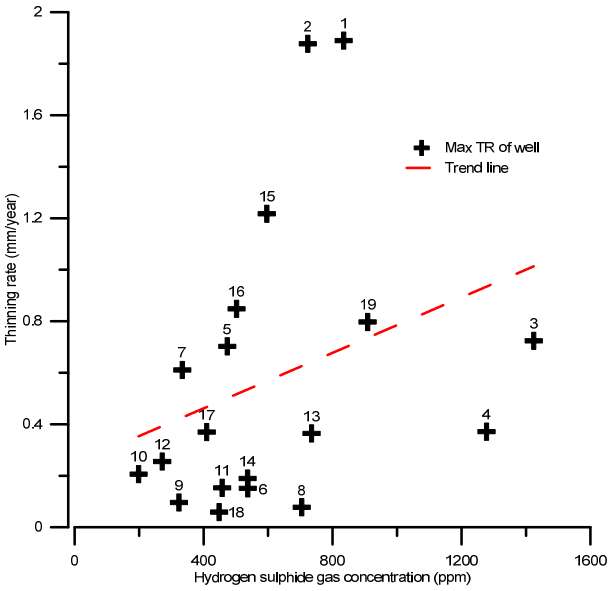

FIGURE 10: Plot of maximum thinning rate with its corresponding H_2S gas concentration

High concentrations of H_2 gas in the wells lead to an increased thinning rate of the casing, as shown in Figure 11. Increased hydrogen concentrations lower the pH of the fluid. The casing experiences stress corrosion cracking at higher concentrations of hydrogen gas. On the other hand, low concentrations of hydrogen gas in the well result in the formation of scales, which protects the casing from the corrosive fluid and slows down corrosion of the casing. Metals become brittle because of the absorption and diffusion of hydrogen at the molecular level. The embrittlement is much more severe when hydrogen sulphide is present (Prasetia et al., 2010).

For two-phase wells, the thinning rate decreased with increased chloride concentrations, but not significantly, as shown in Figure 12. The parameter estimate of chloride in case 4 was also too small to have an effect on the reduction of the thinning rate, compared to the impact of hydrogen sulphide gas.

There was a small decline in the trend on the plot. The chloride ion breaks the passive film formed in the metal, which results in pitting. An increasing trend in the thinning rate was expected. However, a reversal in this trend could be attributed to the use of particular data sets from wells with low pH and low chloride concentrations. Downhole simulation of the chemistry of the fluid led to the observation of increasing chloride concentrations as the fluid flows upward with a corresponding decrease in the fluid pH. The regression results imply that the trend of the thinning rate is independent of the chloride concentrations but is dependent on the fluid pH of the well studied.

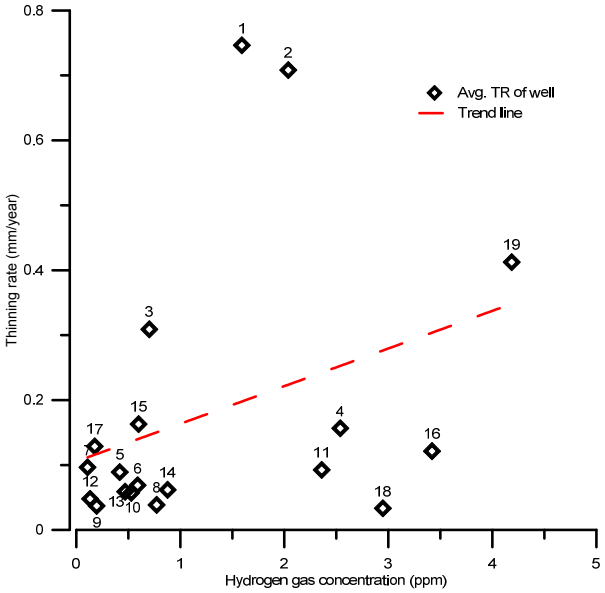

FIGURE 11: Plot of average thinning rate of the casing with minimum H_2 gas concentrations in each well

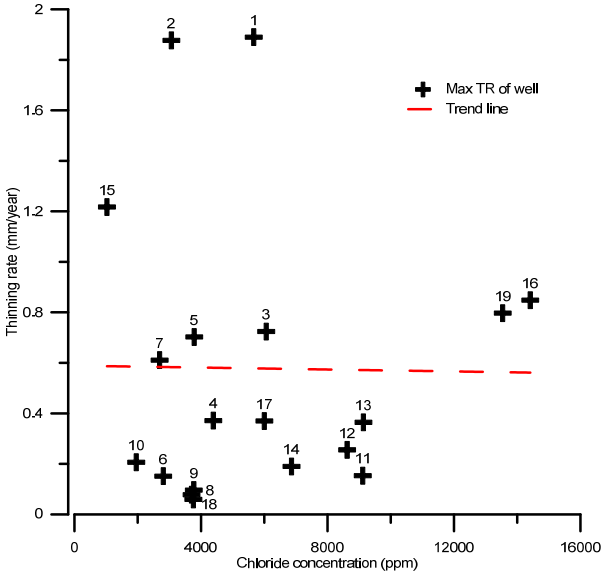

FIGURE 12: Plot of maximum thinning rate with its chloride concentration

The maximum thinning rate of the studied wells with the corresponding sulphate concentrations is plotted in Figure 13. An increase in the thinning rate is evident, based on the results of the regression model for case 4. Fluid with high sulphate concentrations and with low chloride concentrations becomes the more aggressive anion in the corrosion reaction. The decrease in pH may be due to higher concentrations of the sulphur species (H_2S and SO_4) in the datasets.

Parameter estimates of case 5 show a different interpretation of the model. Here, they show that all corrosive species are significant in the model. The CO_{2g} and H_2S_g have high contributions to the thinning rate of the casing. However, in the water phase, the decreasing concentration of CO_{2w} and increasing concentration of H_2S_w, results in an increased thinning rate. The trend of the thinning rate was plotted, based on the maximum and average thinning rates of the casing of each well, as shown in Figures 14 and 15. The increased concentration of dissolved CO_2 in the water contributes to the development of scales, such as calcium carbonate, which shields the casing from corrosion. Fluid, with a low concentration of dissolve CO_2 in the water but with an increasing concentration of dissolved H_2S in the water, contributes to the thinning of the casing. The presence of H_2S inhibits the formation of an oxide film on the steel surface (Banas et al., 2007).

According to Lichti et al. (1981), geothermal fluids with significant concentrations of H_2S and CO_2 often experience the formation of thick adherent layers of corrosive products. This film of corrosive products consists of iron sulphides; the growth rate of these sulphides is directly related to the rate of corrosion. The thinning of the casing becomes apparent when these corrosive products are removed.

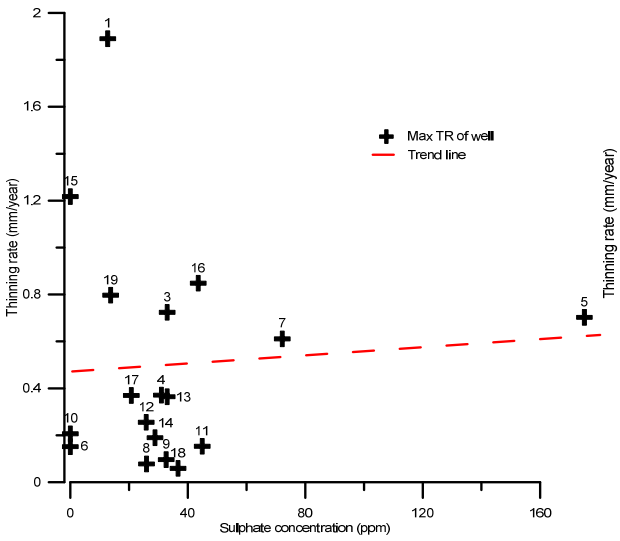

FIGURE 13: Plot of maximum thinning rate with its sulphate concentration

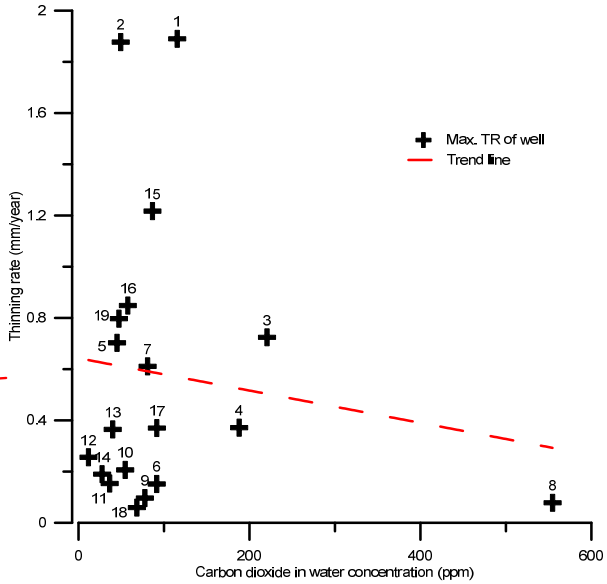

FIGURE 14: Plot of maximum thinning rate with its dissolved CO_2 concentration in water

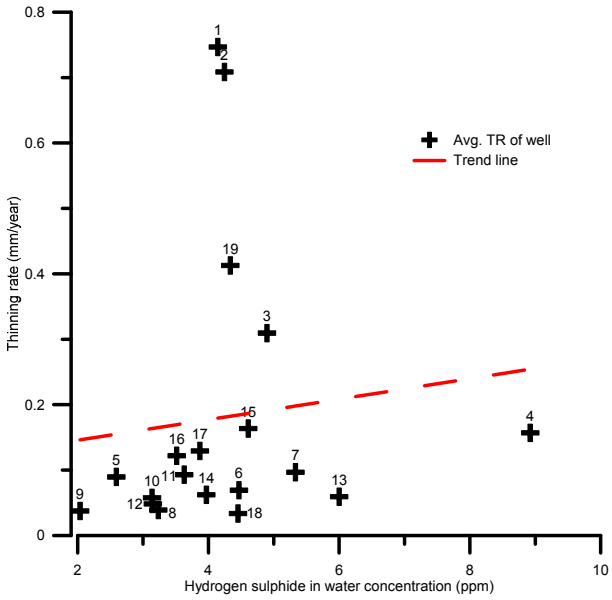

FIGURE 15: Plot of average thinning rate with minimum H_2S concentration in water of each well

Case 6 of the regression showed that temperature significantly affects the thinning rate of the casing, followed by TSS and then well geometry. The coefficient of the determination for case 6 is very low, which shows that there are other factors contributing to the thinning rate of the casing for dry wells. In some geothermal fields, the presence of volatile chloride in steam severely corrodes equipment such as well casings, the wellhead, pipeline and turbines (Hirtz et al., 1991). Even when no traces are found at the surface, it is possible that low pH fluid condensates corrode the casing of most dry wells.

The results of the mean absolute percentage error and the adjusted R^2 of the regression model are shown in Table 11. Of the three cases, case 3 suggests the best model because it has the highest adjusted R^2 and the lowest MAPE. Case 6 of the regression model has a high MAPE value, as expected for a low adjusted R^2. This shows that the model is limited and is lacking other variables that control the thinning rate of the casing. Concerning the regression of corrosive species in predicting the thinning rate, case 4 results have a higher adjusted R2 than case 5, but case 5 has a lower MAPE than case 4.

For choosing the better of the two models, the Akaike information criterion (AIC) was used; AIC is a measure of the relative quality of a statistical model for a given set of data. AIC provides a mean of model selection, and deals with the trade-off between actual data and how well the model fits with the actual data: the lower the value of AIC, the better the fit. The AIC is defined as:

TABLE 11: Mean absolute percentage error (MAPE) and adjusted R^2 of regression model

Case model	Adjusted R^2	MAPE
1	0.5240	170.78
2	0.5561	170.41
3	0.5671	166.76
4 (reduced form)	0.5459	209.50
5	0.4358	149.81
6	0.1634	213.77

$$AIC_i = -2logL_i + 2V_i \tag{19}$$

where L_i = Maximum likelihood for the candidate model *i*;
V_i = Free parameters.

The AIC rewards descriptive accuracy through maximum likelihood and penalizes lack of parsimony according to the number of free parameters, as shown by Equation 19 (Wagenmakers and Farrell, 2004).

The reduced form of case 4 results in lower AIC values, which illustrates a good fit between the predicted values and the observed values, as shown in Table 12.

TABLE 12: Result of Akaike information criterion (AIC) validation between reduced form of case 4 and case 5

Case model	Degree of freedom	AIC
4 (reduced form)	7	-3921.94
5	9	-1504.5

Figures 16-18 show plots for the observed thinning rate of the casing and the predicted value of the thinning, using the affecting factors and the corrosive species for two-phase wells and dry wells. The plots show that the observed thinning rates of two-phase wells are scattered for wells with low pH fluid.

Most of the predicted values for case models 3 to 5 were unable to match the wells with low pH fluid. In addition, the predicted value for some of the wells did not fit the observed values for wells that were mechanically clearing obstructions.

The coefficients of the parameter estimates, listed in Tables 9 and 10, were used to develop a set of linear regression equations for the thinning rate of geothermal casings.

Case 3:

$$Ln(TR) = 23.4251 - 3.0741Ln(T) - 0.7261Ln(V_s) - 4.5885Ln(pH) + 0.3005Ln(X) + 0.0529Ln(f(\theta)) \tag{20}$$

Case 4 (reduced form):

$$TR = 0.04718 - 0.00001Cl_w + 0.0003SO_{4w} + 0.0511H_{2g} + 0.0003H_2S_g + -0.00001CO_{2g} \tag{21}$$

A second set of caliper surveys for Wells 1 to 3 were used to compare the predicted thinning rate, using case models 3 and 4. The average thinning rate of the casings from these surveys was compared with the average predicted thinning rate of the casings.

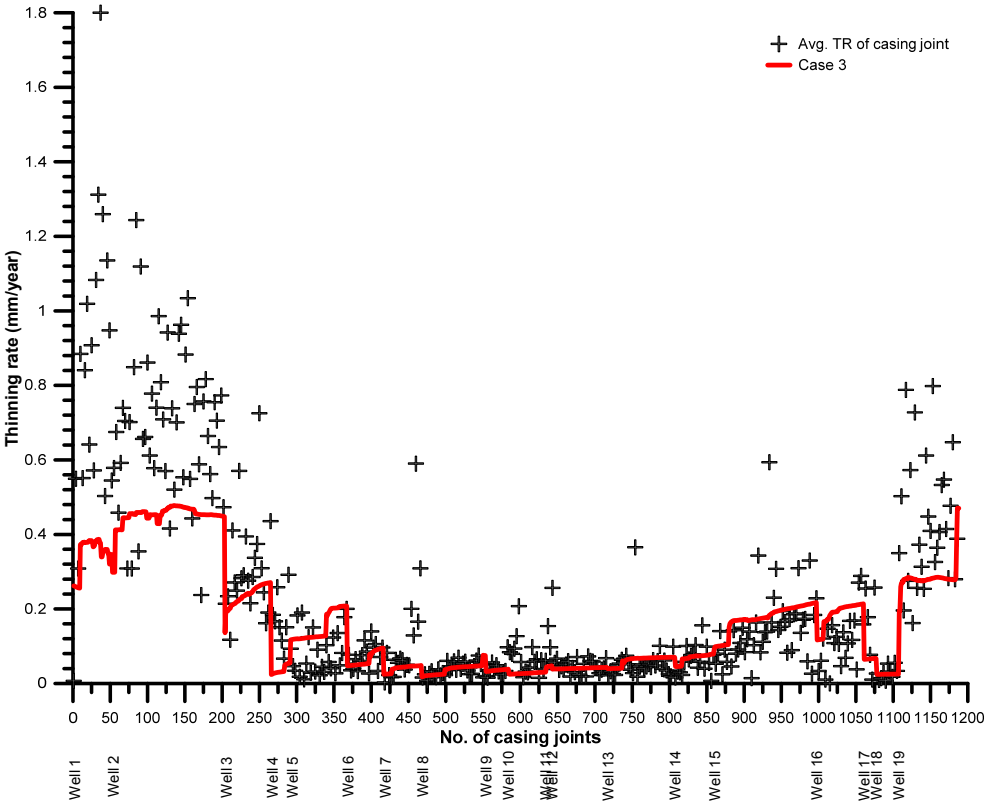

FIGURE 16: Plot of observed and predicted thinning rate, using case 3 model

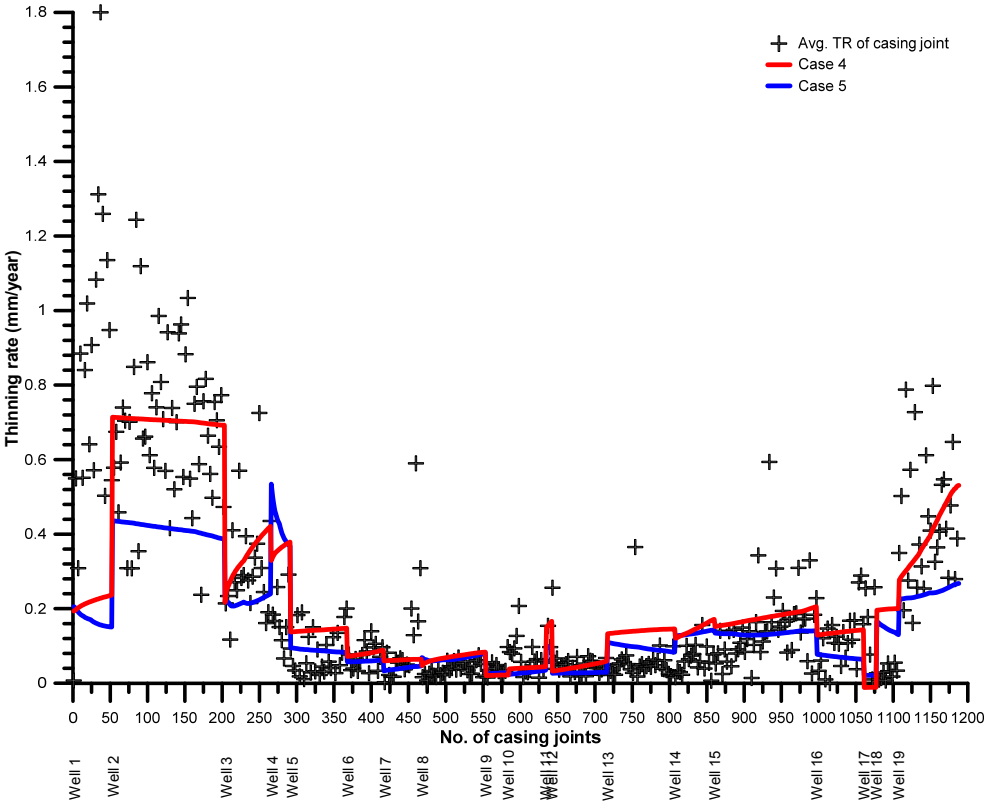

FIGURE 17: Plot of observed and predicted thinning rate, using case 4 and 5 models

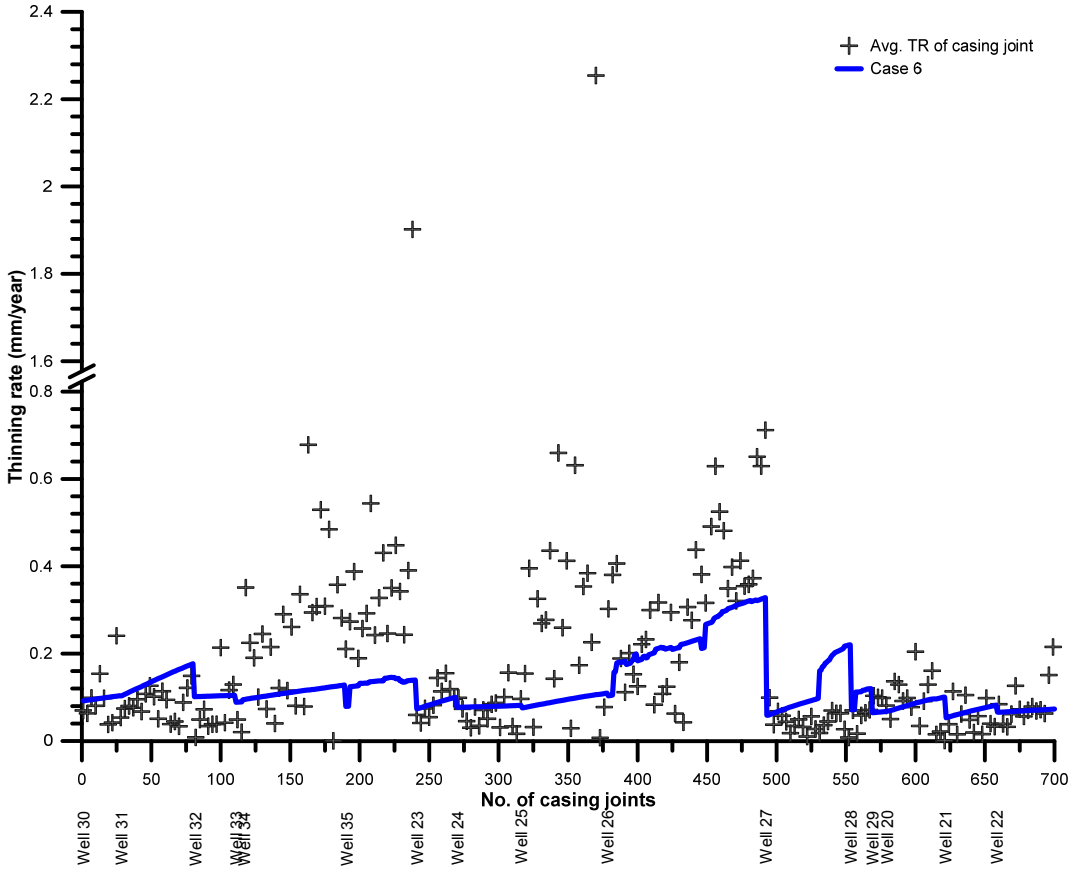

FIGURE 18: Plot of predicted value against observed value of thinning rate for case 6

Reduced case 4 in Well 3 almost predicted the average thinning rate of the caliper surveys, shown in Figure 19. Wells 1 and 2 have large differences between the measured and the predicted average thinning rate of the casing. This was expected, since the predicted value of the regression did not match the observed value in the regression model plot.

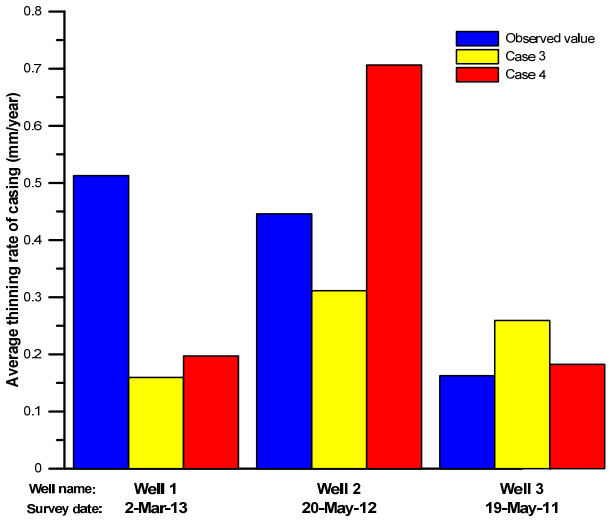

FIGURE 19: Bar chart of average casing thinning rates of measured second caliper surveys and average predicted thinning rate of Wells 1 to 3

Comparing the first and second surveys, the change in the thinning rate for the three wells shows a similar trend in the predicted thinning rate of the casing, using case 3 and 4 models, shown in Figure 20. Even the average predicted thinning rate of the case model did not match the observed average thinning rate from the caliper survey. Despite this, the model can be used as a tool for determining candidate wells to be surveyed. Knowing the thinning rate trend of the casings for specific wells, (based on results from the prediction model), those wells with a high risk of corrosion should be monitored more frequently. Moreover, mitigating actions should be performed on those wells in order to alleviate the high risk associated with their utilization.

The model regression of case 6 was used to predict the average thinning rate of the dry wells, shown in Figure 21. The predicted average thinning rate of the casing conforms to the observed average thinning rate of Wells 21 and 24. These wells showed good matches on the regression model plots, as shown in Figure 18. Well 26 had a low predicted value against the measured value. However, the thinning rate trend between the first and second surveys in the model prediction for dry wells was similar to the regression model for two-phase wells.

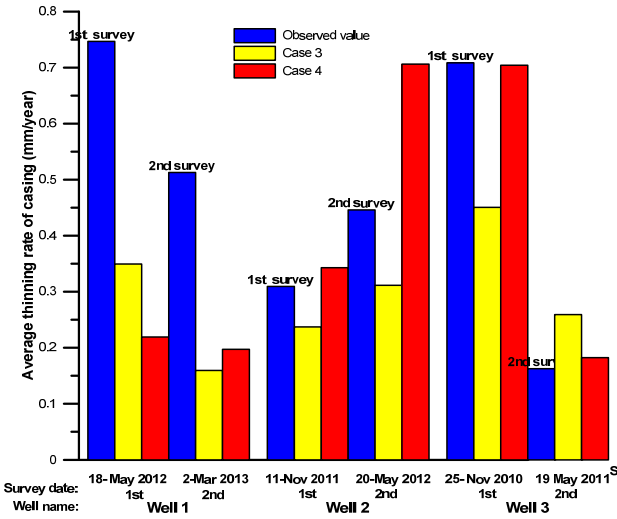

FIGURE 20: Comparison of the average casing thinning rate of the observed and predicted rates of the first and second surveys for Wells 1 to 3

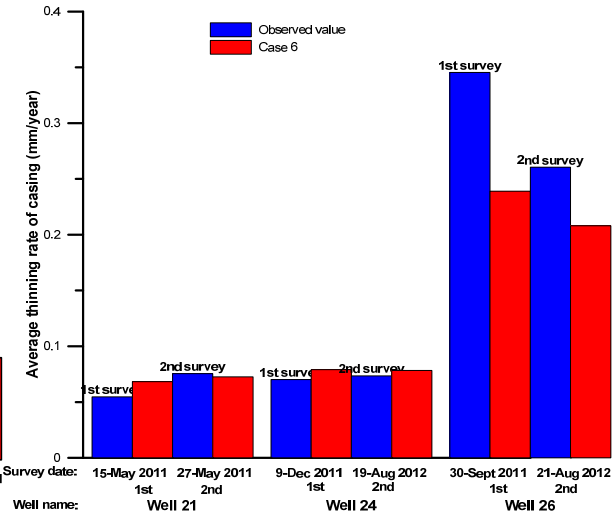

FIGURE 21: Comparison of the average casing thinning rate, both measured and predicted, of the first and second surveys for dry Wells 21, 24 and 26

6. SUMMARY AND CONCLUSIONS

Monitoring the thinning rate of the geothermal well casing is essential in managing the geothermal production field. The loss of integrity of the casing due to thinning could result in high risk in operational safety, environmental damage and loss of profit. The main cause of thinning of the casing is its exposure to fluid discharge.

Regression modelling was used to study the thinning rate of geothermal casing in Leyte Geothermal Production Field. Using software HOLA and WATCH, field data, such as fluid discharge measurements and samples of fluid chemistry from the wellhead, were simulated to obtain the downhole condition. The simulated data were used as datasets for the regression model of the thinning rate of the casing. The results of caliper inspection surveys, conducted on the well casings, were used as response variables in the regression model.

The regression analysis showed that fluid discharge characteristics such as temperature, velocity, pH, steam fraction and the geometry of the well are highly significant on the thinning rate of the geothermal casing for two-phase wells. These factors contribute 56.71% on the thinning of the casing. The prediction of the thinning rate of casings for dry wells, using temperature, fluid velocity, concentration of total suspended solids and the geometry of the well, was found to be significant to the model, but these factors contributed only 16.34% to the thinning of the casing.

The model was inadequate for accurately predicting thinning of the casing. Other factors needed to be considered in order to improve the reliability of the model for predicting casing thickness in dry wells.

The effects of corrosive species, such as $Cl_w, H_2S_w, SO_{4w}, CO_{2w}, H_{2g,}H_2S_g, CO_{2g}$, were also studied. Regression results on the thinning rate, using the concentrations of corrosion species, showed that these corrosion species contributed from 43.6 to 54.7 % to the thinning of the casing. An additive and a multiplicative term of the corrosive species were also included in the regression. The regression models of corrosion species used the Akaike Information Criterion (AIC) in order to select a good model for prediction. Based on the results of the selection test, and using the different models, the additive term of the corrosion species provided a good prediction model for the thinning rate of the casing.

Among the corrosion species considered, H2S and H_2 gases have a significant effect on the thinning of the casing. The presence of these corrosion species in high concentrations could cause hydrogen embrittlement and sulphide stress cracking for wells with high temperature ranges. High sulphate concentrations were present in two-phase wells with a high thinning rate. This illustrates the contribution of sulphur species (H_2S and SO_4) in the thinning of the casing, correlating to a decrease in fluid pH in most of the wells studied.

The study revealed the behaviour of thinning of the casing, comparing regression modelling of the measured thinning rate to the simulated downhole condition. The following were the observed behaviours of the thinning rate:

- Fluid pH predominantly controls the thinning rate of the casing. A low pH geothermal fluid results in a high thinning rate of the casing.
- The thinning rate of the casing increases as the steam fraction of the fluid increases. It is more severe when casing is exposed to acidic geothermal fluids.
- Most of the maximum thinning rates of the well casings included in this study occurred at lower velocity ranges. This could be due to the fluid's long residence time with which to react with the casing.
- A complex well geometry could result in fluid turbulence that can cause an increase in the thinning rate. However, the effect of well geometry is low, based on the data coming from the wells included in this study. Flow turbulence greatly affects the rate of thinning of the casing when fluid pH is low.
- For the temperature range of 188°C to 280°C, the average thinning rate of the casing decreased as the temperature range of the wells increased. A change in the chemistry of reservoir fluid with high sulphate content as it flashed and moved to the surface, yielding a low pH discharge, might be responsible.
- Concentrations of total suspended solids significantly affect the thinning of the casing in dry wells.

The regression model needs further refinement before it can provide accurate predictions of a casing's thinning rate. The model reflects low pH wells. The model should be tested on high pH wells, in order to validate the model further and to test its reliability in predicting the thinning rate of casings. In the meantime, the model can be used to determine if a casing's thinning rate is increasing or decreasing, which can then be used as a criterion for selecting wells for casing inspection.

The condition of the casing before it was installed in the borehole could be responsible for the low coefficient of determination (adjusted R^2) of the regression model. The well stimulation activities conducted on some of the wells included in this study have a significant bearing on the results of the regression modelling.

In order to mitigate an increase in the thinning rate, the following measures are recommended:

- The application of a corrosion and scaling inhibitor;
- The use of corrosion resistant metal alloy for areas with low pH fluid;
- The application of an anti-corrosion chemical coating agent to the casing;
- The application of cathodic protection.

7. RECOMMENDATIONS AND FUTURE WORK

The model was not tested on wells with high pH, due to the unavailability of a repeat survey or data from a high pH two-phase well. Therefore, the model needs to be validated, using new field data from wells with high pH fluid, in order to determine the reliability of the model for predicting the casing-thinning rate. The regression model for the thinning rate should be applied to data from other geothermal fields in order to compare the results with that from the Leyte geothermal production field.

The regression model needs to be improved by segmented linear regression to increase the predicting capability of the model, in which independent variables are partitioned into intervals, for example grouping the data according to low pH and high pH. The effects of partial pressure of CO_2 and H_2S on the thinning rate can be include in the regression model, upon which most studies of corrosion rates in oil and gas are concentrated. Shear stress analysis of the fluid flow to the casing can also be a future focus of the study. The shear stress on the wall surface induced by flowing fluid can prevent film formation or may destroy the protective film that has formed.

Historical data of fluid discharge could be used to monitor changes in the thinning rate of the casing with time.

ACKNOWLEDGMENTS

The author would like to express his deepest gratitude to the following:

... the UNU-GTP family under the dedicated and esteemed staff of Dr. Ingvar Birgir Fridleifsson (retired), Mr. Lúdvík S. Georgsson, Director of UNU-GTP, Mr. Ingimar Gudni Haraldsson (Project Manager), Ms. Málfrídur Ómarsdottir (Environmental Scientist), Ms. Thórhildur Ísberg, and Mr. Markús A. G. Wilde. Thank you for giving me the opportunity to attend the six months training programme and to gain more knowledge about the geothermal industry.

... to his supervisors, Dr. Einar Jón Ásbjörnsson, Mr. Hörður Halldórsson, Mr. Benedikt Steingrímsson and Mr. Halldór Örvar Stefánsson, for guidance and support in completing the research study.

... to Mr. Halldór Ármannsson, Mr. Finnbogi Óskarsson and Dr. Jón Örn Bjarnason, for their support in explaining the behaviour of the corrosion species and their assistance in using software WATCH.

… to Mr. Sverrir Thórhallsson for his opinions regarding corrosion in geothermal wells.

… to the management of Energy Development Corporation: President Richard B. Tantoco; and Senior Vice-President of Technical Services Sector, Manuel S. Ogena, for giving me the opportunity to take part in the training programme.

… to his superiors: Mr. Francis Xavier M. Sta. Ana, Mr. Dave Yglopaz and Mr. Edson Emoricha: thank you for nominating the author to take up this specialized course to enhance his technical capabilities on his present line of work.

… to Mr. Jaime Jemuel Austria for his advice in making the research project.

… to his colleagues: Sir Richie Angcoy, Sir Danny Dacillo, Mam Kat Belas-Dacillo, Regina Cabahug, Jansell Jamero, Gary Mondejar, Hazel Colo, Rowena Abapo, and Suzette Labao for providing the data needed for the study, even with their heavy workloads.

… to his parents, Mr. Armando C. Ponce and Mrs. Aurora S. Ponce, and to his siblings for their love and emotional support, inspiring the author to give his best in everything he does.

… to the UNU fellows for all the memories in the training and wonderful experiences that were shared in Iceland.

…finally to GOD for HIS blessings for all of us.

REFERENCES

Angcoy, E., 2010: *Geochemical modelling of the high-temperature Mahanagdong geothermal field, Leyte, Philippines.* University of Iceland, MSc thesis, UNU-GTP, report 1, 79 pp.

Arason, Th., Björnsson, G., Axelsson, G., Bjarnason, J.Ö., and Helgason, P., 2003: *The geothermal reservoir engineering software package ICEBOX, user´s manual.* Orkustofnun, Reykjavík, report, 48 pp.

Björnsson, G., Arason, P., Bödvarsson, G.S., 1993: *The wellbore simulator HOLA. Version 3.1. User's guide.* Orkustofnun, Reykjavík, 3 pp.

Banas, J., Lelek-Borkowska, U., Mazurkiewics, B., and Solarski, W., 2007: Effect of CO_2 and H_2S on the composition and stability of passive film on iron alloys in geothermal water. *Electrochimica Acta, 52,* 5704-5714.

Cabahug, M.R.S., and Angcoy, E.C. Jr., 2013: Modeling the reservoir fluids of acidic geothermal wells in Mahanagdong, Leyte, Philippines. *Procedia Earth & Planetary Science, 7,* 105-108.

Conover, M., Ellis, P., and Curzon, A., 1979: Material selection guidelines for geothermal power systems. An overview. In: Casper, L.A., and Pinchback, T.R. (eds.), G*eothermal scaling and corrosion.* American Society of Testing Materials, Philadelphia, PA, 262 pp.

Elguedri, M., 1999: Assessment of scaling and corrosion problems in the Kebili geothermal field, Tunisia. Report 1 in: *Geothermal Training in Iceland 1999.* UNU-GTP, Iceland, 1-40.

Finnie, I., Stevick, G.R. and Ridgely, J.R., 1992: The influence of impingement angle on the erosion of ductile metals by angular abrasive particles. *Wear*, *152*, 91-98.

Hirtz, P., Buck, C., and Kunzman, R., 1991: Current techniques in acid-chloride corrosion control and monitoring at the Geysers. *Proceedings 16thWorkshop on Geothermal Reservoir Engineering, Stanford University, Stanford, Ca*, 83 pp.

Ikeuchi, J., Sanada, N., Asano, O., Kurata, Y., Odawara, O., and Okahara, Y., 1982: Corrosion and erosion-corrosion of iron based alloys in a geothermal resource area (Onikobe) in Japan. *Proceedings of the International Conference on Geothermal Energy, Florence, Italy, 1,* 383-394.

Karlsdóttir, S. and Thorbjörnsson, I., 2012*: Hydrogen embrittlement and corrosion in high temperature geothermal well.* NACE international – The Corrosion Society, website: *www.nace.org/ctsm/store/product.aspx?id=cd5f691f-82ed-e111-ac69-0050569a007e*

Lichti, K., Soylemeszoglu, S. and Cunlife, K., 1981: Geothermal corrosion and corrosion products. *Proceedings of the New Zealand Geothermal Workshop 1981*, 103-108.

Lichti, K., White, S. and Sanada, N., 1998: Corrosion in deep and acidic geothermal wells. *Proceedings of the 19thPNOC-EDC Geothermal Conference,* 199-212.

Ocampo-Diaz, J., Valdez-Salaz, B., Shorr, M., Saucesa-M, I., and Rosas-Gonzales, N., 2005: Review of corrosion and scaling problems in Cerro Prieto geothermal field over 31 years of commercial operations. *Proceedings of the World Geothermal Congress 2005, Antalya, Turkey*, 5 pp.

Petric, G., and Ksiazek, P., 1997: Flow-accelerated corrosion in industrial steam and power plants. *Proceedings of the Engineering & Papermakers Conference 1997,* 1537-1542.

Prasetia, A.E., Salazar A.T.N. and Toralde, J.S.S., 2010: Corrosion control in geothermal aerated fluids drilling projects in Asia Pacific. *Proceedings of the World Geothermal Congress 2010, Bali, Indonesia*, 7 pp.

Sanada, N., Kurata, Y., Nanjo, H. and Ikeuchi, J., 1995: Material damage in high velocity acidic fluids. *Geothermal Resources Council, Trans. 19,* 359-363.

Sanada, N., Kurata, Y., Nanjo, H., Ikeuchi, J. and Kimura, S., 1998: Corrosion in acidic geothermal flows with high velocity. *Proceedings of the 20thNew Zealand Geothermal Workshop,* 121-126.

Wagenmakers, E-J., and Farrell, S., 2004: AIC model selection using Akaike weights. *Psychonomic Bulletin & Review*, 2004, 192-196.

Wahl, E, 1977: *Geothermal energy utilization*. Wiley & Sons, Inc., NY, 26-43.

APPENDIX I: Summary of calliper surveys conducted and water and gas chemistry in two-phase wells in the Leyte geothermal field

TABLE 1: Summary of the calliper survey conducted in two-phase wells of Leyte geothermal production field

Well name	Survey date	Years in service (ref. to date survey)	No of casing joints	Size of production casing (mm)	Casing thickness (mm)	Average thinning rate (mm/year)
Well 1	18-May-12	1.05	52	244.475	11.99	0.7467
Well 2	24-Nov-11	1.40	151	244.475	11.05	0.7086
Well 3	25-Nov-10	1.40	62	177.8	9.19	0.3094
Well 4	14-Jan-12	6.69	26	177.8	9.19	0.1569
Well 5	23-Nov-10	8.05	76	244.475	11.99	0.0895
Well 6	1-Feb-12	14.21	49	339.725	12.19	0.0691
Well 7	14-Jun-12	14.57	51	244.475	11.05	0.0967
Well 8	5-Dec-10	12.72	86	177.8	9.19	0.0390
Well 9	8-Dec-10	12.56	31	244.475	11.05	0.0375
Well 10	27-Nov-10	13.02	50	244.475	11.05	0.0575
Well 11	11-Sep-12	14.97	8	244.475	11.05	0.0929
Well 12	18-Jan-11	13.14	74	244.475	11.05	0.0483
Well 13	5-Sep-11	14.75	91	244.475	11.05	0.0592
Well 14	17-Dec-12	18.09	53	244.475	11.99	0.0622
Well 15	12-Aug-11	5.09	137	244.475	11.99	0.1634
Well 16	12-Dec-12	8.09	63	244.475	11.05	0.1218
Well 17	9-Sep-12	3.47	17	244.475	11.05	0.1291
Well 18	13-Aug-12	12.88	30	244.475	11.05	0.0336
Well 19	26-Aug-12	1.28	81	177.8	9.19	0.4127

TABLE 2: Summary of calliper survey conducted in dry wells of Leyte geothermal production field

Well name	Survey date	Years in service (ref. to date survey)	No of casing joints	Size of production casing (mm)	Casing thickness (mm)	Average thinning rate of cas. joints (mm/year)
Well 20	30-Nov-11	13.98	42	244.475	11.05	0.1033
Well 21	15-May-11	28.30	37	177.8	9.19	0.0547
Well 22	3-Dec-11	12.41	42	244.475	11.05	0.0869
Well 23	21-Aug-11	12.74	29	244.475	11.05	0.1099
Well 24	9-Dec-11	13.04	47	244.475	11.05	0.0701
Well 25	1-Mar-11	1.70	62	244.475	11.05	0.2895
Well 26	30-Sep-11	2.67	114	244.475	11.05	0.3455
Well 27	3-Sep-11	14.81	61	244.475	11.99	0.0481
Well 28	15-Aug-11	15.00	15	339.725	12.19	0.0529
Well 29	26-Feb-11	13.13	11	244.475	11.99	0.0829
Well 30	8-Jun-12	12.94	27	244.475	11.05	0.1118
Well 31	14-Dec-10	11.68	53	244.475	11.05	0.0906
Well 32	19-Dec-12	13.48	30	244.475	11.05	0.0641
Well 33	14-Oct-11	13.18	5	339.725	12.19	0.0458
Well 34	21-Nov-10	4.46	74	244.475	11.99	0.2483
Well 35	4-Feb-12	2.87	51	244.475	11.99	0.3608

TABLE 3: Sampled water chemistry of two-phase wells in Leyte geothermal production field

Well name	Sampling date	Wellhead pressure	Sampling pressure	Enthalpy	pH	Surface concentration (ppm)														
						Li	Fe	HCO3	SO4	Cl	F	Ca	Mg	K	Na	SiO2	B	NH3	H2S	CO2 Total
Well 1	6-May-12	1.01	0.991	1742	3.5	12	16	0	14.6	6495	1.5	238	5.6	947	3327	1188	25	18.5	3.18	0
Well 2	20-Aug-12	1	1	2399	3.6	5.5	62	0	1727	3157	2.4	14	45	315	2400	543	78	33.1	1.08	0
Well 3	29-May-10	1.08	1.06	2265	3.4	14	71	0	40.7	7479	0	191	8.5	1005	3864	1120	53	70.2	0.68	0
Well 4	7-Jun-09	1.03	0.95	1822	5.1	10	1.8	0	35.8	5064	0	101	0.6	741	2561	909	29	38.3	2.17	47.8
Well 5	19-Jan-11	1.03	0.87	1558	4	7.5	1.2	0	188	4066	0	40	2.8	458	2324	632	39	18.8	2.03	0
Well 6	15-Jul-10	1.26	1.23	1232	6.7	0	0	23.8	0	2933	0	47	0	291	1694	583	43	0	0	22.6
Well 7	26-Sep-12	1.2	1.082	1078	7.3	5.6	0.1	54.7	77	2870	1.9	14	0.1	288	1703	603	48	2.53	2.76	50.2
Well 8	1-Jun-10	1.29	1.14	1441	5.9	8.7	0	28.8	32.3	4603	0	86	0	504	2715	707	50	2.79	1.78	50.7
Well 9	1-Jun-10	1.24	1.12	1222	5.6	7.5	0	22.8	34.9	4035	0	21	0	440	2349	618	50	3.62	1.47	75.3
Well 10	3-Sep-08	1.393	1.383	1115	6.1	0	0	44.5	0	1953	0	5.3	0	170	1195	461	23	0	0	79.2
Well 11	23-Jun-12	1.41	1.41	1539	5.8	21	0.3	7.26	45.1	9151	1.5	190	0.3	1024	4987	646	218	4.17	5.19	32.1
Well 12	10-Feb-11	1.37	1.29	1264	6.8	20	0.2	14.6	25.7	8573	2	178	0	945	4601	655	188	2.88	0.57	20.2
Well 13	29-Oct-11	1.4	1.395	2476	6.2	24	1.5	25	34.2	9475	2.9	214	1.1	986	4836	632	221	4.83	4.61	20.8
Well 14	26-Apr-12	1.19	1.052	1212	7	16	0.7	8.62	31	7375	1.8	123	0.3	784	3952	593	185	2.8	3.92	6.93
Well 15	13-Jun-11	1.66	1.4	1409	4.8	0	1.1	12.2	0	1128	0	29	0.2	134	563	0	56	7.68	60.8	382
Well 16	25-Jul-12	1.5	1.453	2463	4.4	31	8.4	0	45	14897	5	275	2	1727	6899	765	663	16.6	10.4	0
Well 17	11-Jan-12	1.73	1.657	1351	5.8	16	0.4	15.3	21.2	6129	1.1	68	0	660	3404	718	150	4.37	3.64	36.9
Well 18	26-Aug-10	1.55	1.5	2536	6.2	8	0.1	28.3	37.9	3884	0	44	0	396	2214	554	161	5.34	0.11	46.1
Well 19	23-Jul-12	1.32	1.129	2370	3.8	34	37	0	14.9	14679	1.8	366	2	1886	7655	817	509	3.32	6.22	0

TABLE 4: Sampled gas chemistry of two-phase wells in Leyte geothermal production field

Well name	Sampling date	WHP	Sampling pressure	Surface concentration (mmol / 100 mol)									
				H	CO_2	H_2S	NH_3	He	H_2	Ar	N_2	CH_4	Na
Well 1	6-May-12	1.01	0.991	1742	610	37.7		0	1.4	0.05	4.5	3.03	25.1
Well 2	20-Aug-12	1.01	0.01	2399	892	38	1.62	0	1.81	0.03	4.08	3.11	54.1
Well 3	29-May-10	1.08	1.06	2265	374	45	1.31	0	0.62	0.02	1.54	0.58	15.1
Well 4	7-Jun-09	1.03	0.95	1822	984	59	41.2	0	2.23	0.54	49.3	3.53	5.32
Well 5	19-Jan-11	1.03	0.87	1558	513	22.4	1.56	0	0.36	0.08	4.44	0.83	40.2
Well 6	23-Aug-10	1.27	1.24	1232	780	25	3.08	0	0.55	0.21	12.2	6.09	708
Well 7	14-Sep-12	1.16	1.082	1078	399	13.2	1.41	0	0.09	0.34	20.7	1.16	290
Well 8	20-Aug-10	1.25	1.16	1441	843	21	1.12	0	0.69	0.06	4.82	1.5	59.5
Well 9	30-Aug-10	1.21	1.06	1222	556	13.2	1.31	0	0.18	0.04	2.8	1.63	143
Well 10	19-Nov-08	1.403	1.393	1088	536	11.6	1.15	0	0.54	0.4	26.8	6.43	1.06
Well 11	23-Jun-12	1.41	1.41	1539	503	23.9	1.38	0	2.14	0.04	3.39	2.09	171
Well 12	10-Feb-11	1.37	1.29	1264	148	15.1	1.56	0	0.12	0.01	0.61	0.05	150
Well 13	29-Oct-11	1.4	1.395	2476	460	38.6	2.05	0	0.42	0.18	13.5	0.28	54.9
Well 14	26-Apr-12	1.19	1.052	1212	183	21.2	1.68	0	0.77	0.17	14.5	0.71	8.28
Well 15	13-Jun-11	1.66	1.4	1409	358	16.8	0.18	0	0.5	0.01	0.99	0.19	35.8
Well 16	25-Jul-12	1.5	1.4	2463	706	26.3	0.86	0	3.06	0.18	17.2	1.14	40
Well 17	11-Jan-12	1.73	1.4	1351	895	20.4	2.46	0	0.16	0	0.32	0.52	45.9
Well 18	26-Aug-10	1.55	1.4	2536	750	23.6	2.92	0	2.63	0.3	24	4.69	13.9
Well 19	23-Jul-12	1.32	1.4	2370	306	35.6	0.53	0	3.66	0.04	2.42	1.06	67.7